New strategies based on microfluidics for the synthesis of metal organic frameworks

Carlos Echaide-Górriz,[1] Coralie Clément,[2] Fernando Cacho-Bailo,[1] Carlos Téllez[1] and Joaquín Coronas[1,*]

[1]Chemical and Environmental Engineering Department and Instituto de Nanociencia de Aragón (INA), Universidad de Zaragoza, 50018 Zaragoza, Spain

[2]Polytech Nantes, Université de Nantes, 44306 Nantes, France

*Corresponding author: Joaquín Coronas, e-mail: coronas@unizar.es.

Abstract

Metal-organic frameworks (MOFs) are highly porous crystalline materials formed by the coordination of organic ligands with metal clusters. Despite the significant progress in their development over the last few years and their applications in various classic and emerging fields, the control of their shape and size remains a challenge, in particular the search for more efficient and environmentally friendly syntheses. In this context, the microfluidics approach allows not only the continuous production of MOFs but also an accurate reaction parameter control in their synthesis, representing a step towards intensification, versatility and scalability in the use of MOFs. This review is devoted to highlighting the multitude of synergies appearing when dealing with MOFs and microfluidics, not only in the bare synthesis of MOFs and their hierarchical structures but also when fabricating hollow fiber membranes with important applications in the separation field.

1. Introduction

Metal-organic frameworks (MOFs) are porous, crystalline materials formed by the coordination of organic ligands with metal clusters. Due to their extremely high specific surface area and uniform porosity, there has been significant progress in their development over the last decade and a half which has seen the appearance of thousands of new MOFs with applications in various classic and emerging fields. These include gas separation and adsorption, catalysis, encapsulation, medicine, and electronics.[1-11] A great deal of effort has been put into the discovery of different MOF based materials with the objective of achieving excellent performances in their corresponding applications. However, it is time to make these versatile materials industrially profitable by controlling their shape and size and making their syntheses more efficient and environmentally friendlier. In this context, the continuous synthesis of MOFs,[12] especially by means of microfluidics,[13] has attracted the attention of the research community in recent years as an alternative to traditional discontinuous batch reactions.[14-21] This approach allows not only continuous production but also an accurate reaction parameter control in the synthesis, providing a step towards intensification, versatility and scalability in the use of MOFs.

In addition to describing the state of the art in microfluidics applied to the synthesis of MOFs, this review aims at putting reported research into perspective. Using information published by others and our own experience,[13, 22-26] we will classify and summarize the different existing approaches to the synthesis of MOFs by using microfluidic tools. In addition, we will suggest future lines towards which the microfluidics-MOF tandem is headed. Microfluidics allows the crystal engineering of MOFs, which is of paramount importance in catalyst and adsorbent design but also for membranes, sensors and other electronic devices whose possible economic development may depend on the availability of efficient and reliable synthetic methodologies. While there are a few published reviews of the continuous flow production of MOFs and related materials,[27-31] none of them fully address the content of our review. In fact,

Zhang *et al*.[27] refer to the use of continuous flow for preparative inorganic chemistry. MOFs are one among several materials, and hierarchical structures and hollow fiber membranes are not addressed. The work by Wang *et al*.[28] deals with the current types of microfluidic devices used in the synthesis of different types of nanohybrids (composed of two or more components that exhibit many distinct physicochemical properties) based on the classification of the four main kinds of materials: metal, nonmetal inorganic, polymer and composites. MOFs are not among the materials studied. The short reviews by Batten *et al*.[29] and Dunne *et al*.[30] present continuous flow reactors as the most versatile method for up scaling the synthesis of MOFs and describe the continuous synthesis of MOFs using microfluidics but also screw extruders mechanochemical synthesis devices. MOF hollow fiber membranes are hardly addressed. Finally, Chen and Shen[31] review membranes in microfluidics tangentially mentioning MOF hollow fiber membranes in the field of gas detection research.

The origin of microfluidics can be related to gas chromatography applications, i.e. to separation applications.[32] This was followed by the development of microfluidic based reaction technologies.[33] In microfluidics the thicknesses of the mass and heat boundary layers (those in which the viscosity affects the layer fluid in the immediate vicinity of the corresponding bonding surface) are closer to the characteristic dimensions (e.g. the internal diameter of the used pipe or the channel width) than in conventional systems. From the point of view of mass and heat transfer in chemical synthesis, the general advantages of microfluidics are:[34] the use of small reagent volumes, reaction selectivity enhancement, lower energy consumption per unit temperature, and faster reactions. These advantages also give rise to intrinsically safer reaction systems with smaller reaction volumes and thus smaller carbon footprints than conventional processes. In addition, when microfluidics is used to prepare MOF-supported hollow fiber membranes, the porous pipe has a double mission: it acts both as reactor and membrane porous support.[24]

It is generally accepted that the characteristic dimension of a microfluidic system is below 500 µm. This value can go up to 1 mm when the system operates at Reynolds (Re, the ratio of the convection to the diffusion mass transport) and thermal Péclet (Pe, the ratio of convection to the conduction heat transport) dimensionless numbers below 250 and 1000, respectively. These values define the microfluidic operation, bearing in mind that mesofluidics is broadly considered for diameters between 500 µm and a few millimeters.[34] Moreover, Re < 250 means a laminar flow regime (always achieved when Re < 2,300) with no axial mixing within the reactor.[34] The laminar regime requires low velocities, i.e. high residence times. These conditions, together with the fact that microfluidic systems have a high surface area to volume ratio, result in efficient operations in terms of both energy and media savings and reaction control and yield.

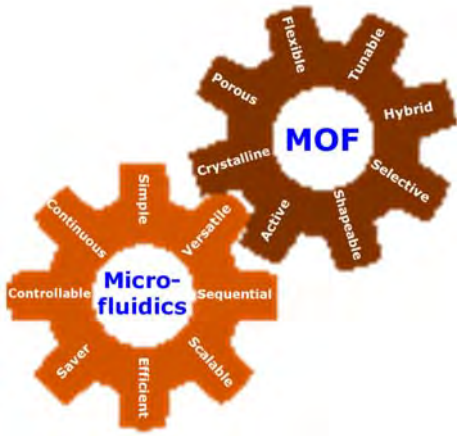

Fig. 1. Combination of the chemical properties and performance possibilities of MOFs with the advantages of microfluidics.

Fig. 1 illustrates the motivation for this monographic study. This lies in the combination of the chemical properties (hybrid character, tuning), structural features (porosity, crystallinity, flexibility) and performance possibilities (shapeability, selective and large adsorption capacity,

catalytic activity) of MOFs with the advantages of microfluidics (simplicity, versatility, possibility of easy sequencing, scalability, efficiency, controllability, continuous operation). We can say that this is currently producing a multitude of synergies. These synergies are related to the bare synthesis of MOFs and MOF hierarchical structures and to the fabrication of hollow fiber membranes, as shown below.

2. Microfluidic synthesis of MOF crystals

2.1. Zeolite synthesis by microfluidics

Zeolites are porous crystalline aluminosilicates that can be considered as the inorganic MOF counterpart. They display similar properties such as extensive porosity, a high degree of crystallinity and high chemical and thermal stability.[2, 35] Both of them have well-defined structural features (cages and pores) at the microporous scale that have made them particularly attractive in the field of gas storage, separation by adsorption and membranes, and heterogeneous catalysis.[3, 19, 36-38]

Due to the demanding synthesis conditions required by zeolites, i.e. high pressure and temperature, the microfluidic system has not emerged as the most suitable for their synthesis.[39] Conventional discontinuous syntheses based on batch reactors are preferred for these crystalline aluminosilicates.[40, 41] Nevertheless, such systems have limitations (inefficient mixing, inhomogeneous temperature distribution, among others) that can be overcome by the microfluidic system.[42] These benefits have been reported in only a few works.[13, 34] The published articles addressing zeolite syntheses accomplished by a microfluidic system are gathered in Table 1. They comprise systems with 500-1000 μm internal diameters of channels and pipes.

Table 1. Summary of the literature regarding zeolite syntheses performed in microfluidic system.

Zeolite	Crystal size (nm)	Pipe diameters (µm)	Residence time (min)	Reactants flow (µL/min)	Type of microfluidic	Temperature (°C)	Ref.
Zeolite A	426	ID: 750 OD: 1200	13.3	~ 200	Single phase	90	[43]
Zeolite A	408	ID: 1000	20	~ 133	Two phase	80	[44]
ZSM-5	380 ± 20	ID: 508	20	2-8	DIM*	150	[45]
Zeolite A	1200	ID: 1000	30	800	Two-phase	90	[46]

***DIM corresponds to droplet- and ionic liquid-assisted microfluidic.**

In 2006, Ju *et al.*[43] reported that the use of a microchannel reactor for the continuous synthesis of zeolite NaA not only reduced the mean particle size and the particle size distribution (PSD) in comparison with the batch system, but also the crystallization time. The latter was reduced tenfold in the case of microfluidics (13.3 min instead of 135 min), helped by the long aging of the solution. In their device, a synthesis mixture containing both precursors was pumped through a microchannel as a single phase. The capillary was immersed in an oil bath which controlled the reaction temperature. However, an enhancement of this continuous flow system had to be carried out to solve the problem of channel clogging, which deemed it unusable, and to fine-tune the control of the PSD. In 2009, Pan *et al.*[44] improved the microfluidic process using a second liquid phase made of paraffin for the preparation of zeolite A. By adjusting a second pump on the original tube, a continuous phase of liquid paraffin was provided, carrying and separating the reaction mixture into droplets (segmented flow). In this manner, the blockage problem was eliminated and the necessary aging time of the solution was substantially reduced. The technique also showed an enhancement of crystal size control due to the mixing intensification taking place inside the droplets. Smaller mean particle sizes and narrower PSD were obtained than in single-phase microfluidic or in conventional batch and microwave-heated reactors. Hoang *et al.*[45] chose to combine ionic liquids and droplet-based microfluidics to achieve the preparation of zeolite ZSM-5. The synthesis of this zeolite

conventionally required high temperatures and long reaction times. Here, the ionic liquid was chosen as a thermally stable and non-volatile template for the construction of the nanostructures while the droplet-microreactors ensured a mixing of the reactants by rapid heat and mass transfer. The products exhibited a uniform morphology as well as a narrow PSD, and the reaction time was significantly reduced from several hours to tens of minutes. The novelty presented by Yu *et al*.[46] compared with the previous approaches was to convey the two precursor solutions at the same time but separately in the microfluidics device, keeping the oil phase for the formation of the droplets. In this manner, the zeolite A hydrogels were prepared continuously in one step. With this process, the adjustment of the silica to alumina flow rate ratios enabled a precise control of the hydrogel composition and therefore a control of the crystallinity and particle size. Despite these achievements in the production of zeolites by microfluidic means, they have been limited by the challenging hydrothermal conditions of synthesis. However, other materials which share common properties with zeolites were found to be more suitable for exploiting the great potential of microfluidics, such as aluminophosphate $AlPO_4$-5[47] and, more interestingly, metal-organic frameworks (MOFs). It should be noted that prior to the synthesis of MOFs using microfluidics, Puigmartí-Luis *et al*.[48] had prepared related materials (coordination polymer nanofibers) using microfluidic technologies.

2.2. MOF synthesis by microfluidics

Hydrothermal and solvothermal syntheses represent the widely used conventional methods for the MOF production. Nevertheless, they suffer from a very long crystallization period (from several hours to days) along with arduous control of the crystal size.[49, 50] From this standpoint, continuous flow processes including microfluidic synthesis appear to be more suited to industrial requirements than typical laboratory-scale batch approaches. Fig. 2 is an illustration

of the time saving achieved with microfluidics in comparison with other common synthesis methods (the shortest time has been picked for each type of synthesis).

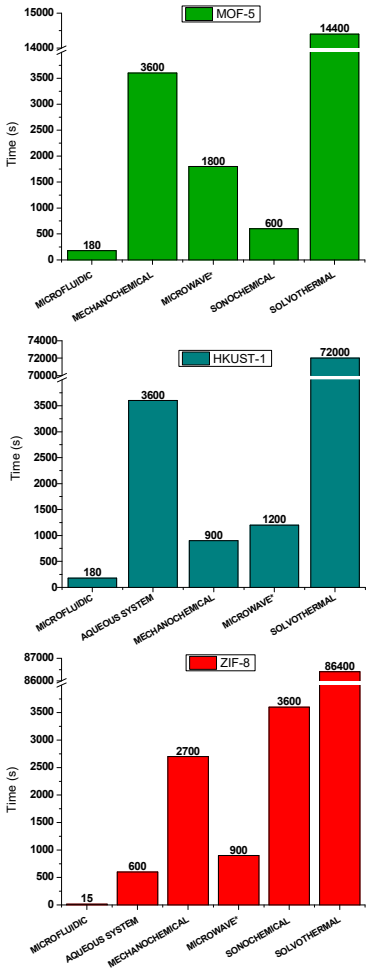

Fig. 2. Comparison of the synthesis time of different common methods of synthesis for three MOFs (MOF-5,[51-55] HKUST-1,[50, 56-59] and ZIF-8[60-63]). *Microwave-assisted solvothermal synthesis.

The majority of reported MOF syntheses by microfluidics have been conducted following a droplet-based strategy similar to that mentioned for zeolites, benefiting from its efficient

mixing.[13, 55, 56, 64] The ligand and metal precursors are usually mixed in a T-junction device which is connected to a tube for the oil carrier. The micro- or nanodroplets are generated from the shear interaction between the oil phase and the mixture, and constitute the segmented phase while the oil acts as the continuous phase. The droplets pass through the tube that is then immersed in a temperature controlled oil bath in order to perform the solvothermal synthesis. After reaction, the synthesized products are collected at the outlet of a cooled vial, avoiding further crystallization. The upper oil phase is separated and the synthesized products are recovered by centrifuging, washing and drying. Table 2 provides an overview of MOF crystal syntheses using microfluidic methodology.

Table 2. Summary of the literature regarding MOF crystal syntheses performed in microfluidic reactor systems (trimesic acid: H_3BTC; ethanol: EtOH; dimethylformamide: DMF; terephthalic acid: H_2BDC; 2-methylimidiazole: Hmlm; methanol: MeOH).

MOF	Molar composition	Crystal size	Pipe diameters (mm)	Residence time (s)	Reactants flow (µL/min)	Temperature (°C)	Ref.
HKUST-1	$Cu(NO_3)_2{\cdot}H_2O$:H_3BTC: H_2O:EtOH:DMF 3:2:555:86:193	5-15 µm	ID: 0.5 OD: 1.5	180	12	90	56
MOF-5	$Zn(NO_3)2{\cdot}6H_2O$:H_2BDC:DMF 3:1:270	10-15 µm		180	1-12	90	
IRMOF-3	$Zn(NO3)_2{\cdot}6H_2O$:H_2BDC-NH_2:DMF 3:1:270	10-15 µm		180	1-12	90	
UiO-66	$ZrCl_4$:H_2BDC:HCl:DMF 1:1:1:80	< 1 µm		900	1-12	90	
Fe-MIL-88B-NH_2	Fe:ligand:DMF:H_2O 1:1:52:52	180 nm	ID: 1.0 OD: 1.6	20	618	95	13
Fe-MIL-88B	Fe:ligand:DMF:H_2O 1:0.7:52:52	520 nm		240	154	95	
Fe-MIL-88B-Br	Fe:ligand:DMF:H_2O 1:1:104:104	680 nm		360	103	95	
ZIF-8	Zn:Hmlm:MeOH:NH_3 1:2:41:30	~ 80 nm	ID: 1.6	15	6000	Room temperature	60
ZIF-8	Zn:Hmlm:H_2O 1:70:197	355 ± 71 nm	ID: 1.6	600	1000	25	64

Faustini *et al.*[55] first reported the successful use of segmented flow for the synthesis of Cu_3BTC_2. Droplets of 200 µm diameter were formed inside the PFA tube and the solvothermal synthesis was pursued at 90 °C. Optical microscopy revealed that the crystalline structure of

Cu_3BTC_2 could be identified only after 1 min of reaction time while 24 h were needed for the conventional solvothermal synthesis at 90 °C. In addition, the measurement of the specific surface area showed crystals with higher quality than in conventional bulk processes.[59, 65, 66] With the same continuous process, they synthesized other MOFs of interest:[56] HKUST-1, MOF-5, IRMOF-3 and UiO-66. Each time, both precursors (ligand and metal) were dissolved in a polar medium and the droplets were then carried by a nonpolar oil. The flow rates were controlled by means of syringe pumps. Different retention times (from 1 to 12 min) and metal concentrations were investigated for HKUST-1 and the optimal retention time was found to be 3 min (at 90 °C), leading to the highest BET specific surface area (S_{BET}). Faustini *et al*. also reported that increasing the reaction time or using a more concentrated precursor decreases S_{BET}. In the case of HKUST-1, the crystals were of higher quality than in conventional solvothermal synthesis. The syntheses of the other MOFs were achieved only after 15 min for UiO-66 and 3 min for MOF-5 and IRMOF-3. Furthermore, the two latter MOFs showed smaller particle sizes (10-15 µm) than in conventional solvothermal synthesis, demonstrating the validity of this ultrafast process. Paseta *et al*.[13] focused on the application of segmented microfluidics to dicarboxylate based MIL-88B type MOFs: Fe-MIL-88B-NH_2, Fe-MIL-88B and Fe-MIL-88B-Br, in order to obtain an acceleration of the crystallization time and show the feasibility of the process. Metal and ligand precursors were dissolved and pumped separately to a mixing-cold zone, after which a third syringe-pump provided silicon oil to form the segmented flow. Using this strategy, an ultrafast synthesis was achieved, especially for Fe-MIL-88B-NH_2 (20 s at 95 °C), but very short residence times were also obtained at the same temperature for Fe-MIL-88B and Fe-MIL-88B-Br, these being 4 min and 6 min, respectively. Particular attention was paid to the shape, size and PSD variations resulting from changes in the residence time. Fig. 3 shows the evolution of the particle size distribution with the residence time. An increase in the latter leads to a larger average particle size and a broader PSD dispersion consequently appears as a function of the residence time. For instance, a residence time variation from 20 s to 600 s resulted in larger crystals: from 160 nm to 900 nm.

A study of the slug volume growth showed the same effects. Shape changes were also observed for the crystals, having a round shape at short times and becoming more angular at longer times. Considering that a precise control of the residence time is highly achievable in microfluidic devices, as well as the dimensions of the slugs, Paseta *et al.*[13] proved that the technique offers an innovative fine-tuning of the mean particle size and PSD.

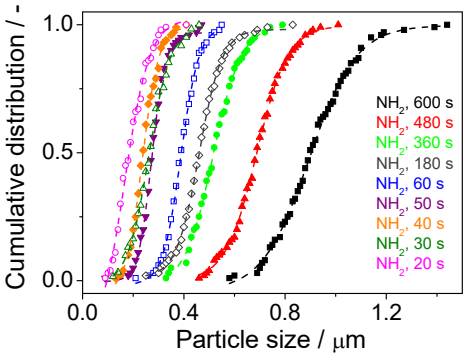

Fig. 3. Cumulative particle size distribution of Fe-MIL-88B-NH_2 synthesized at 95 °C after several residence times.[13]

A continuous process using microfluidic conditions developed by Polyzoidis *et al.*[60] showed the potential tuneability and upscaling of ZIF-8 synthesis. In their setup, the mixing of precursor solutions was implemented in a T-type micromixer. They were then continuously fed in a helically wound residence time capillary for the reaction at room temperature. The investigation of different solvents led the authors to conclude that only the use of aqueous ammonia and methanol for the zinc nitrate and 2-methylimidazole, respectively, allowed the production of pure ZIF-8 with short residence times. Indeed, the N_2 adsorption measurements showed a product of excellent quality with a S_{BET} of 1770 m^2/g obtained at a residence time shorter than 15 s. It is worth noting that the quality of the produced material remained stable even with a variation of the residence time or the reagent concentrations, proving the solidity of this synthesis. For the fastest reaction, a production rate of 640 $g \cdot day^{-1}$ was achieved

corresponding to a high space time yield of 210,000 $kg \cdot day^{-1} \cdot m^{-3}$, which was unprecedented for MOFs at that time. The quantitatively and qualitatively feasible production of ZIF-8 demonstrated here, in addition to the characteristic repeatability of the continuous process, makes possible the use of this method at a larger scale. Recently, Kolmykov *et al.*[64] have proposed a more environmentally-friendly synthesis for the same MOF, replacing the organic solvent with water alone or a biphasic flow made up of an oil phase and water droplets. In the latter case, a second T-micromixer was added to provide the oil phase. A heated section was also positioned after the precursor mixing. For the monophasic continuous synthesis, high flow rates (30-240 $mL \cdot h^{-1}$) were used in order to avoid the sedimentation of the crystals in the microreactor. Varying the oil composition, the authors found a correlation between the oil viscosity and the steps of nucleation and growth of the nanocrystals. Larger particles were produced with the use of silicon oil than with n-decane or 1-octadecene, and their sizes seemed to be little influenced by the increase in temperature. The authors demonstrated that the high viscosity of the silicon oil corresponded to significant pressure in the channel that was responsible for the particle size increase and the temperature inhibition. For both monophasic and biphasic flow syntheses, crystals of high quality were produced, showing the same S_{BET} as the previous continuous synthesis with organic solvent (ca. 1700 $g \cdot m^{-2}$). The syntheses were relatively fast with a residence time of 10 min, and the variation of the experimental parameters (flow rates, temperature, etc.) enabled the synthesis of crystals over a wide size range.

The microfluidic synthesis process not only addresses the simple production of MOF crystals, but also allows variations and evolutions responding to different needs and applications. Microfluidic pen lithography (MPL) successfully performs the highly reproducible synthesis of homogeneous MOFs at a precise location. The HKUST-1 synthesis is a representative example of the MPL procedure:[67] a femtoliter droplet of solvent DMSO solution containing $Cu(NO_3)_2 \cdot 2.5(H_2O)$ is generated on a SiO_2 surface by means of a first microfluidic stylus after which a femtoliter volume of trimesic acid in DMSO solution is placed within the droplet with a

second pen. A premature solvent evaporation of the patterned droplet is avoided by the control of the relative humidity of the chamber. The accurate handling of the pen lithography technique allows the creation of nanoscale MOF arrays: for example, a 30 × 30 droplet array with a droplet distance of 20 µm for HKUST-1 synthesis.

Digital microfluidics combines droplet-based microfluidics and electrowetting for achieving the generation of single MOF crystals in a highly automated way (Fig. 4). A fluid reservoir provides mother droplets containing MOF precursors. The bottom plate of the path followed by the mother droplets is made of actuation electrodes and a dielectric layer. An electric field established in this layer at one side of the droplet creates an imbalance of the interfacial tension, inducing motion in the mother droplets. In the top plate, hydrophilic micropatches were designed in the hydrophobic matrix. Their selective wettability enables the printing of femtoliter droplets from the mother droplets. The top plate is then removed and the single crystals are collected after evaporation of the solvent. Witters *et al.*[68] applied their device to the printing of HKUST-1 single crystals. The use of 20 µm × 20 µm micropatches resulted in uniform size crystals (5.3 ± 0.9 µm) with a high-throughput production of 1600 femtoliter droplets printed per second. Such technology providing single MOF crystals may facilitate their study at a single-crystallite level and also improve their applications. Some pure structural MOF crystals have already been integrated in a sensing system for alcohol and organophosphate pesticides.[69-71] Nevertheless, few examples have been reported.

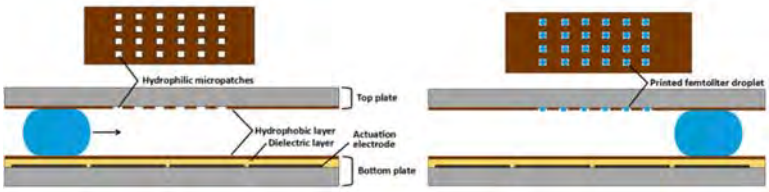

Fig. 4. Digital microfluidics scheme.

Post-synthetic modification (PSM) appears to be a promising method to broaden the potential of MOF crystals. The introduction of a relevant functional group may lead to an improvement in the chemical and physical properties, as proved by the functionalization of UiO-66 for hydrogen sulfide, oxidative agents and DNA detections. For this purpose, Jambovane *et al*.[72] directly integrated the functionalization step in the droplet-based microfluidic process, saving time, cost and energy at the same time. Functionalization of UiO-66-NH_2 in UiO-66-NH-$COCH_3$ and UiO-66-NH-FITC was conducted with the addition of the reagent containing the functional group (acetic acid or fluorescein isothiocyanate (FITC), respectively) in a modulator, whose role was to enhance the control of the particle size. Metal salts, organic ligand and the modulator were injected separately but simultaneously into an oil phase to merge and form droplets for the production of both functionalized MOFs in this one-pot synthesis.

Another droplet-based technology has tried to raise MOF production to a large-scale industrial level. Interestingly, the spray-drying technique developed by Maspoch *et al*.[73] eliminates the separation and drying steps which considerably increase the production time. A mixture of metal ions, organic ligand and solvent is sprayed in small droplets through a nozzle in a hot gas stream leading to instantaneous MOF crystallization and evaporation of the solvent. One of the advantages of spray-drying is that the process is suitable for already existing industrial spray dryers. It is worth mentioning that the as-obtained MOFs had particularly small dimensions; in fact, they were ca. 5 μm spherical hollow particles constituted by assembled MOF nanoparticles.

In line with the last example, the possibility of using microfluidics to obtain MOFs with hierarchical pore structures is also interesting. This is of paramount importance when there is some intracrystalline diffusion limitation in catalysts and adsorbents but also when the handling of powders is inconvenient due, for instance, to pressure drop problems in beds or to safety concerns when respirable aerosols are produced.[74] To overcome these drawbacks, hierarchical porous structures were addressed in the past mainly with zeolitic materials.[75] In general, these

hierarchical structures with micro/mesopores, meso/macropores and micro/macropores have been successfully prepared by controlling the synthesis conditions.[74, 76]

Several approaches have been reported to obtain by microfluidics MOFs as hierarchical structures, such as template free synthesis strategies, ligand extension, microemulsion methods, nanocrystal self-assembly and the use of different surfactants.[77] In particular, thin layers of MOFs have been shaped as hollow capsules using a biphasic synthesis mixture comprising two immiscible solvents, each containing one of the two MOF precursors.[78] After achieving the emulsification, crystallization takes place only at the liquid-liquid interface. In fact, the metal aqueous solution flows through a tapered capillary (110 μm inner diameter) centered in the reactor tube (760 μm inner diameter μm), and the ligand organic solution flows around it (Fig. 5A). This mechanism causes the thickness (1.5-2 μm) of the film to be uniform and has been used to produce hollow capsules of MOF [$Cu_3(BTC)_2$] with uniform diameter of around 375 μm (Fig. 5B). This interfacial reaction has also been carried out to produce functional bio-MOF (MIL-88A) hollow spheres with controlled size in the 35-2000 μm range with architectures from single-shell to double-shell (a hollow capsule inside another hollow capsule).[79] Finally, Zhang *et al*. have recently used the microfluidic jet spray drying technology to reassemble nano-sized MIL-101 into hierarchical structures for benzene adsorption,[80] in line with the above mentioned strategy discovered by Carné-Sánchez *et al*.[73]

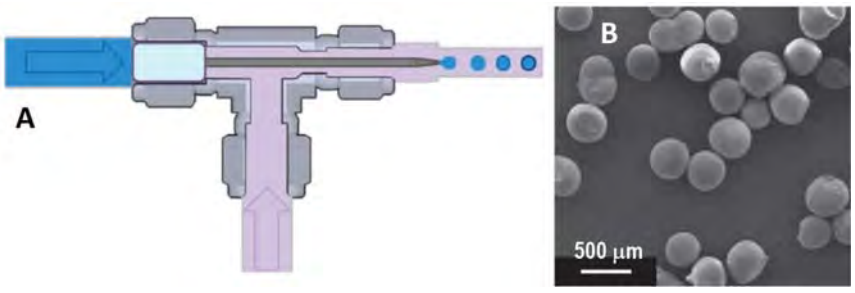

Fig. 5. T-junction showing details of the microfluidic emulsification (A). SEM image of hollow MOF [$Cu_3(BTC)_2$] capsules (B).[78]

4. MOF-based membranes

4.1. Introduction

The methods of microfluidic synthesis allow an accurate control of MOF PSD during their synthesis, thus the reactants and solvent usage can be dramatically reduced.[34] Microfluidic systems also offer similar advantages to the synthesis of MOF-based membranes where the layer thickness is the parameter to be controlled. This synthesis technique takes place necessarily on hollow fiber membrane supports, which act as a pipe and a reactor at the same time. The advantages of hollow fiber membranes, as compared to flat and typical tubular membranes, lie fundamentally in their high volumetric areas of up to 10,000 m^2/m^3 (compared to the ca. 1,000 m^2/m^3 of flat membranes).[24, 81] For this reason, hollow fibers can be considered the most practical membrane geometry in terms of membrane packing efficiency,[82] which is of paramount importance for developing commercial membrane applications.[83]

Based on previous works where the formation of continuous MOF films was carried out on inorganic and polymeric supports, various strategies have been developed since the publication of the first microfluidics approach reported by Brown *et al*. in 2014.[84] These strategies include the use of different materials as hollow fiber supports (polysulfone, polyimide, polyamide, PVDF and even metals) where different MOFs have been synthesized (ZIF-8, ZIF-7, ZIF-9, ZIF-9-III, ZIF-93, SIM-1/ZIF-94, among others). The combinations obtained will be explained below.

Brown *et al*. designed the so-called IMMP (interfacial microfluidic membrane process) method for the synthesis of a continuous ZIF-8 film on the lumen of a Torlon® (polyamide-imide) hollow fiber.[84] Eum *et al*. analyzed the chemical and physical mechanism of this method, and

suggested a few synthesis modifications to optimize both the film thickness and the membrane performance when separating H_2/C_3H_8 and C_3H_6/C_3H_8 mixtures.[85, 86] Finally, Marti *et al*.[87] used a variation of the IMMP method already studied by Brown *et al*.[84] to synthesize a ZIF-8 layer on the outer surface of a hollow fiber.

Cacho-Bailo *et al*. developed their own microfluidic method to synthesize ZIF-8 and ZIF-7 on the lumen side of a polysulfone hollow fiber.[24] Afterwards, they achieved the formation of a ZIF-93 layer,[22] a ZIF-9 layer and the combination of ZIF-9 with either ZIF-8 or ZIF-63 on polyimide P84® hollow fiber supports.[26] Besides, they published a study about the annealing effect on ZIF-8 and ZIF-93 based P84® hollow fibers, leading to a significant improvement in the performance of these membranes.[23] Cacho-Bailo *et al*. also prepared by microfluidics a ZIF-9 continuous layer on the inner surface of a metallic (Ni) hollow fiber.[25] The microfluidic approach allowed an *in situ* crystalline transition, by pumping pure water through the hollow fiber, of the ZIF-9 to the ZIF-9-III dense phase, more suitable for separating H_2/CO_2 mixtures.

Analogously, Biswal *et al*.[88] and Mao *et al*.[89] carried out the crystallization of layers of ZIF-8 and Cu-BTC on both the inner and the outer surfaces of PBI-BuI hollow fibers and of HKUST-1, respectively. In this case, the synthesis was carried out by a novel method in which the source of metal for the crystallization was a layer of copper hydroxide nanostrands deposited by a previous microfluidic filtration stage.

New ideas for process intensification strategies are being sought by industry and the scientific community to produce the most energy-efficient model possible. In this context, membrane technologies represent one of the strategies for improving current separation technologies.[90, 91] Hollow fiber membranes in particular are the perfect candidates for optimizing performance vs. cost across a wide range of the industry spectrum without the need for disruptive changes.[92] The works published to date have shown the usefulness of hollow fiber membranes for performing strategic gas separation processes related to mixtures containing olefins and paraffins but also pre- and post-combustion streams.[22-24, 26, 84-86, 93-96]

4.2. Previous work

In the last decade, several methods have been developed to synthesize continuous MOF layers on different supports (Fig. 6). The first works were carried out on flat ceramic supports. Arnold *et al.*[97] in 2007 achieved the formation of a continuous manganese formate layer on porous α-alumina and graphite discs by *in situ* crystallization. Both supports had to be pretreated to increase the presence of carbonyl, carboxyl and hydroxyl groups, which allowed a proper MOF growth. The results of the study did not include gas separation or permeance measurements, but the authors included an in-depth study about the crystallinity and morphology of the layer, as well as the characteristics of the interactions between MOFs and the support.

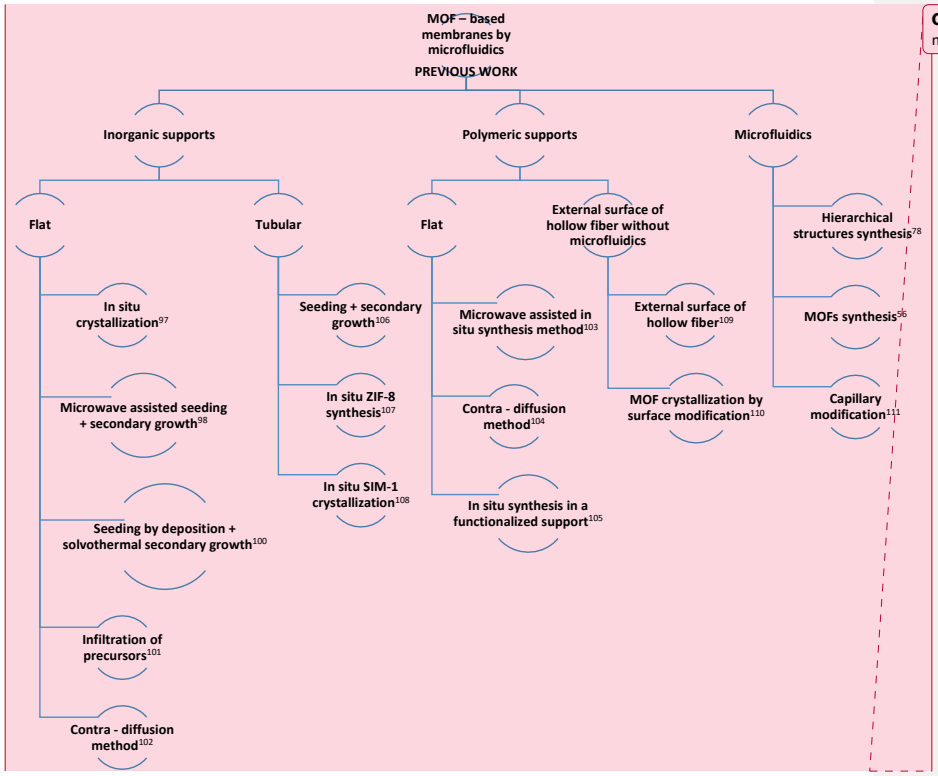

Comentado [JC1]: Revisar el primer texto "MOF-based…" que no se corte con las líneas tampoco

Fig. 6. Map of the previous work of the synthesis of MOF-based membranes by microfluidics.

Bux *et al*.[98] published in 2009 the first work about microwave assisted seeding with a secondary growth. ZIF-8 was chosen to form the continuous film on a titania porous support. They used the modified ZIF-8 synthesis in methanol developed by Cravillon *et al*.[99] in 2009, instead of the original recipe with DMF because the former solvent is easier to remove from the structure after the synthesis than the latter. The results showed interesting permeances through the membrane of different gases such as hydrogen, oxygen, carbon dioxide, nitrogen and methane. Besides, this membrane showed a H_2/CH_4 selectivity of 11.2 at 298 K, considerably above the Knudsen selectivity factor (2.8). In the same year, Liu *et al*.[100] achieved the formation of a continuous MOF-5 layer on α-alumina porous discs by seeding and secondary growth. Moreover, Li *et al*.[101] and Hara *et al*.[102] developed new methods to synthesize intergrowth layers of ZIF-8 on inorganic supports involving infiltration and contra-diffusion, respectively.

Centrone *et al*.[103] in 2010 were the first authors to form MOF-based membranes on flat polyacrylonitrile (PAN) supports by microwave-assisted synthesis. Even though they did not achieve the formation of a continuous MOF layer, this publication marked the beginning of a new research field. Later on, other authors used new methods to synthesize continuous layers of MOFs on flat polymeric supports. For instance, Yao *et al*.[104] in 2011 carried out further research into the contra-diffusion method to synthesize ZIF-8 continuous films on nylon supports, while Meilikhov *et al*.[105] achieved the formation of this composite by conventional *in situ* crystallization.

The first MOF composite membranes synthesized on tubular supports appeared in 2010.[106, 107] In fact, Xu *et al*.[108] developed a method to synthesize a continuous ZIF-8 layer from a concentrated synthesis gel on the outer surface of a ceramic hollow fiber support with an outer diameter of 2 mm. And MOF-based membranes were synthesized on the outer surface of a hollow fiber support for the first time by Brown *et al*.[109] in 2012. In this work, the ZIF-90 was

homogeneously crystallized on Torlon® hollow fibers of 400 µm diameter for gas separation applications. Two years later Li *et al*.[110] synthesized by *in situ* growth Cu-BTC and ZIF-8 on the outside of functionalized PAN hollow fiber supports.

Finally, a few authors have tried the deposition or synthesis of MOFs on the inner wall of capillary columns for open tubular capillary electrochromatography (OT-CEC). Xu *et al*. (see Fig. 6) reported the *in situ* synthesis of MIL-100(Fe) on fused-silica capillary columns of 75 µm inner diameter and 41.2 cm effective length through the layer-by-layer self-assembly approach.[111] Besides, Li *et al*. published in the same year a method to coat polymethyl metracrylate capillary columns for OT-CEC with previously prepared MOF CAU-1 particles.[112] However, according to Yu *et al*., these two approaches were either uncontrollable methods or else a thin MOF layer was formed through many cycles. In consequence, they designed a new method to coat the inner wall of fused-silica capillary columns (75 µm inner diameter) with ZIF-90 crystals for OT-CEC.[113] The method consisted of direct covalent bonding between functionalized MOF particles and the capillary wall. Here, ZIF-90 was employed as a model MOF because of its textural properties and the aldehyde groups present in its structure, which allowed covalent functionalization with amine groups, i.e. with 3-aminopropyltriethoxysilane (APTES). It is important to highlight that in this method the MOF layer was not synthesized *in situ*, but formed by pumping a suspension of MOF particles (previously crystallized and functionalized) through the lumen of the capillary column.

4.3. Synthesis methods and gas permeation results

4.3.1. Interfacial microfluidic membrane processing method

As indicated, Brown *et al*. were the first to report the synthesis of MOF-based membranes by microfluidics in 2014.[84] They designed a method to synthesize ZIF-8 continuous layers on the inner or outer surfaces of Torlon® hollow fiber supports. This consisted of the

diffusion of two solutions, each with a different ZIF-8 precursor as solute (Zn^{2+} and 2-methylimidazole (HmIm)), through the hollow fiber thickness. For this purpose, the surfaces of the hollow fiber (sealed in a membrane module) were in contact with either the Zn^{2+} or the HmIm solutions as follows (see Fig. 7): the solution on the lumen side was pumped with a peristaltic pump, while that on the shell side of the module was stagnant. The method consisted of pumping through the bore side one of the solutions during 120 min at 10 $\mu L \cdot min^{-1}$, after which it was kept stagnant for 210 min; the solution was pumped again during 20 min at 10 µL/min and finally it was kept stagnant again for 210 min.[84] This method was called interfacial microfluidic membrane processing (IMMP). Additionally, two parameters were studied: the location of each precursor solution (lumen or shell side), and the miscibility between the two solvents used. Consequently, the total combinations were eight, although only the five cases considered most interesting were studied. In case 1, the precursors were fed in immiscible solvents: the metal salt was dissolved in water and fed through the bore side of the hollow fiber, whereas the ligand HmIm was dissolved in 1-octanol and added at the shell side of the membrane module. In cases 2 and 3, the Zn solution was fed through the lumen and shell sides, respectively, but both precursor solutions were dissolved in the same solvents: water in case 2 and 1-octanol in case 3. In these three cases, the MOF continuous layer was synthesized on the inner surface of the hollow fiber, although a sharp interface between the MOF layer and the polymer could be observed only when both solvents were immiscible (case 1). However, when both solvents were miscible the resultant layer was 10 µm deep inside the porosity of the support. In cases 4 and 5 the precursors were also dissolved in the immiscible solvents. In case 4, the Zn was dissolved in water and fed and located at the shell side, whilst in case 5 the metal salt was dissolved in 1-octanol and also fed through the shell side. As the authors hypothesized, the result of changing the metal solution (limiting reactant) was that the MOF layer was synthesized on the outer surface of the hollow fiber. In spite of obtaining a composite layer in

the 5 different cases, Brown *et al*. only characterized case 1 by measuring the H_2/C_3H_8 and C_3H_6/C_3H_8 mixture separation performances.[84]

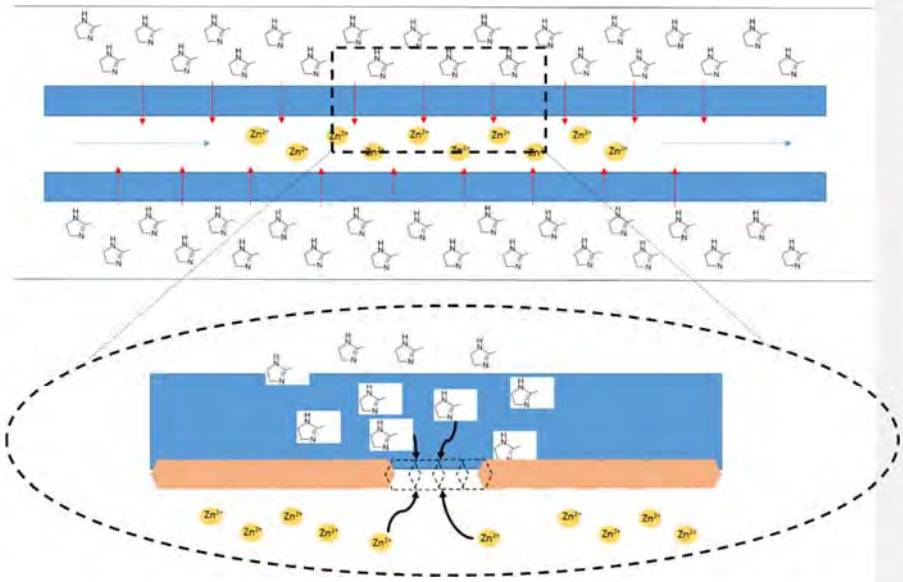

Fig. 7. IMMP method scheme. Zn^{2+} solution pumped through the hollow fiber lumen (blue), and the Hmim molecules diffusing from the shell side to the hollow fiber inner surface. When both MOF precursors react, they form the crystals (pink) along the inner surface.[84]

Brown *et al*.[84] observed a clear sieving effect when separating the mixture H_2/C_3H_8 at 120 °C (130 ± 8 separation factor), although a higher than expected C_3H_8 permeance was measured. This prevented a high C_3H_6/C_3H_8 separation factor (2.2 ± 0.4) at 25 °C. The explanation for this result was the bypass detected during the separation process. As the authors mentioned, the gas mixture feed could permeate through the cross-section area of the entrance, avoiding the selective MOF layer. When this was covered with PDMS, the membrane selectivity increased significantly and the C_3H_8 permeance notably decreased, which meant higher separation factors (the values in Table 3 correspond to those obtained with the PDMS pretreatment). Additionally,

Brown *et al.*[84] demonstrated the high stability of their composite membrane by separating H_2/C_3H_8 and C_3H_6/C_3H_8 mixtures in a long term test (35 h). With single gas measurements they proved that in the as-made membrane 60% of the flow of C_3H_8 occurred through the bypass, 37% through defects and only 3% through the ZIF-8 membrane. When using the PDMS sealed membrane, the bypass contribution was null, but still 92% of the molar flow was through membrane defects. Consequently, from the authors' point of view, the IMMP method needed to be improved to reduce the presence of defects.

Table 3. Separation performances of the MOF-based hollow fiber membranes synthesized by microfluidics. The given values are the permeance in GPU of the smallest gas of each pair, and the separation factor (α). The temperatures in brackets correspond to those of the testing conditions

MOF	H_2/C_3H_8 (120 °C)		C_3H_6/C_3H_8 (25 °C)		H_2/CH_4 (35 °C)		H_2/CO_2 (35 °C)		He/C_3H_8 (35 °C)		N_2/CO_2 (25 °C)		Ref
	H_2	α	C_3H_6	α	H_2	α	H_2	α	He	α	N_2	α	
ZIF-8	750	370	27	8	-	-	-	-	-	-	-	-	84
ZIF-8	3000	1850	33	17.5	-	-	-	-	-	-	-	-	86
ZIF-8	2250	3000	0.4	180	-	-	-	-	-	-	-	-	85
ZIF-8	-	-	-	-	-	-	-	-	-	-	22	52	87
ZIF-8	-	-	-	-	-	-	-	-	2	8	-	-	88
ZIF-8	-	-	-	-	51.8	17.2	49.5	2.6	-	-	-	-	24
ZIF-7	-	-	-	-	15.4	34.6	15.6	2.4	-	-	-	-	24
ZIF-8	-	-	-	-	-	-	126.9	4.1	-	-	-	-	26
ZIF-67	-	-	-	-	-	-	38.7	3.6	-	-	-	-	26
ZIF-93	-	-	-	-	27.2	60	-	-	-	-	-	-	22
ZIF-9	-	-	-	-	-	-	101.0	4.8	-	-	-	-	
ZIF-8/ZIF-9	-	-	-	-	-	-	72.9	5.2	-	-	-	-	26
ZIF-67/ZIF-9	-	-	-	-	-	-	29.6	5.4	-	-	-	-	26
SIM-1	-	-	-	-	-	-		0.25*	-	-	-	-	94
ZIF-9-III	-	-	-	-	-	-	102*	22.2*	-	-	-	-	94
CuBTC	-	-	-	-	-	-	-	-	0.5	9	-	-	88
HKUST-1	-	-	-	-	6003	2.5	6003	4.2	-	-	-	-	89
ZIF-90	-	-	-	-	1084	1.1	1084	50	-	-	-	-	96

***Results at 0 °C.**

Comentado [JC2]: Falta la referencia. Es la 26?

Eum *et al.*[86] conducted an in-depth study of the synthesis mechanism of the IMMP method previously published by Brown *et al.*[84] They observed the role of the reactants transport, film crystallization and the hollow fiber support porous structure, analyzing three different cases. In the first case, Eum *et al.*[86] reproduced the IMMP method several times and took samples of the composite membrane at different times to observe the morphology of the cross section area. They could distinguish a dual MOF layer at the end of the first stage of the IMMP

synthesis (which consisted of pumping the metal solution for 120 min) formed by a dense film followed by a discontinuous MOF layer on the top. The dual layer, caused by different linker availability with time, was homogenized after the next 210 min stage. Eum *et al*.[86] identified this stage as crucial for the formation of a defect free MOF layer, since the C_3H_6/C_3H_8 separation performance was greatly enhanced. The final two stages increased the thickness of the homogeneous dense layer and at the same time the separation performance of the hollow fiber membranes. In the second case, as Eum *et al*.[86] hypothesized, an increase in ZIF-8 crystallization during the first stage would create a denser film that would impede further crystallization, so the final thickness would decrease. To achieve a thinner and defect free layer, the module was heated at 40 °C for the first 30 min and then stabilized at 30 °C after a slow cold ramp, creating the so called non-isothermal IMMP method. The results demonstrated the validity of this hypothesis, since the final thickness decreased somewhat from 10 ± 2 μm to 9 ± 2 μm while the membrane performance barely changed. In the third case, the IMMP method followed was the same as in the second case, but Eum *et al*.[86] increased the average pore size of the hollow fiber support from 290 nm to 480 nm to improve the MOF-polymer adherence and thus make the MOF layer thinner. Once the ZIF-8 layer was synthesized on this new support by the non-isothermal IMMP method studied in case 2, they measured a MOF layer thickness of 5 ± 1 μm, giving rise to separation factors of about 1850 and 17.5 in the case of the H_2/C_3H_8 and C_3H_6/C_3H_8 mixtures, respectively (see Table 3). These performances were the highest achieved in this study: the low MOF layer thickness allowed a higher C_3H_6 permeance, and the low C_3H_8 permeance gave rise to a high C_3H_6/C_3H_8 separation factor. Additionally, Eum *et al*.[86] measured dry and wet He permeabilities to detect the presence of defects. Large defects such as cracks or pinholes are usually detected in wet conditions, but these were not found in any of the three cases. However, nanoscopic defects (below 20 nm), that can be detected in dry conditions, were evidenced in case 1, but not in cases 2 and 3.

Eum *et al*.[85] published another work regarding the synthesis of a continuous ZIF-8 layer on the lumen of Torlon® hollow fibers by adding two new modifications to the non-isothermal IMMP synthesis method. These allowed the membrane to achieve C_3H_6/C_3H_8 separation factors of 180 at 0 bar as the transmembrane pressure differential ΔP and 25 °C, very close to the ideal separation factor based upon adsorption and diffusion parameters, and 90 ± 6 at ΔP = 8.5 bar and 25 °C. The first consisted of the modification of the hollow fiber porosity: a more open porous structure led to a more uniform linker diffusion during the MOF layer formation, helping to create a defect-free layer. In such conditions, the authors observed by SEM an overgrowth of MOF structures inside the new high-porous hollow fiber cross section, thus they decreased the linker concentration by a factor of two to reduce the penetration into the bore side, and therefore the MOF formation rate. As seen in Table 3, the improvement in permeance and selectivity when separating C_3H_6/C_3H_8 was significant compared to those obtained in the previous publications by the same group.[84 86] Nevertheless, the MOF layer thickness, 8.1 ± 1.6 µm, was higher than the minimum they had previously achieved (5 ± 1 µm).[86] The lack of large defects in the ZIF-8 layer gave rise to the good performances achieved when measuring H_2/C_3H_8 and C_3H_6/C_3H_8 equimolar mixtures (see Table 3).

More importantly, Eum *et al*.[85] studied the C_3H_6/C_3H_8 separation performance of the ZIF-8 based membrane at different ΔP (from 0 to 8.5 bar), showing high separation factors even at high pressure, as mentioned above (90 ± 6 C_3H_6/C_3H_8 separation factor at ΔP = 8.5 bar and 25 °C). This performance was explained by the fundamental characteristics of transport in nanoporous structures.

Marti *et al*.[114] synthesized in 2017 a ZIF-8 continuous layer on the outer surface of a Torlon® hollow fiber. Their synthesis method was based on the IMMP developed by Brown *et al*.,[84] which was demonstrated to be capable of forming the MOF layer on the outer surface of the hollow fiber by changing the location of the metal salt solution.[84] However, Marti *et al*. used water as solvent for both ZIF-8 precursors; in consequence the resultant ZIF-8 layer had two

regions, in agreement with Brown *et al*.:[84] a denser layer on the top of the support, and a more porous one inside its microstructure. It was more interesting to use miscible rather than immiscible solvents because, as they hypothesized, the layer region inside the hollow fiber porosity contributed to a good anchoring, counteracting the delamination of the MOF film. They also studied the flow ratio between metal and linker solutions to control the thickness of the MOF layer inside the support microstructure and the layer on its outside (dense layer).[114] High metal/linker flow ratios led to a layer with no thickness inside the microstructure, poor mechanical properties and difficulties when handling due to its fragility. The best membrane, synthesized with a metal/linker flow ratio of 0.25/0.13 (mL/min), was able to separate CO_2/N_2 with a separation factor of 52, showing a CO_2 permeance of 22 GPU (see Table 3).

4.3.2. *In situ* crystallization method

The synthesis method developed by Cacho-Bailo *et al*.[24] dealt with the *in situ* crystallization of ZIF-8 or ZIF-7 on the inner surface of a polysulfone hollow fiber support by pumping the two precursor solutions through the bore side, which led to extra savings compared to the Brown *et al*. strategy (Fig. 8). The ZIF-8 layer was synthesized by mixing solutions of Zn^{2+} and HmIm in methanol. The ZIF-7 was synthesized by mixing solutions of Zn^{2+} and benzimidazole (bIm) in ethanol. In this case the membrane was tested by separating equimolar mixtures of H_2/CH_4 and CO_2/CH_4, among others.

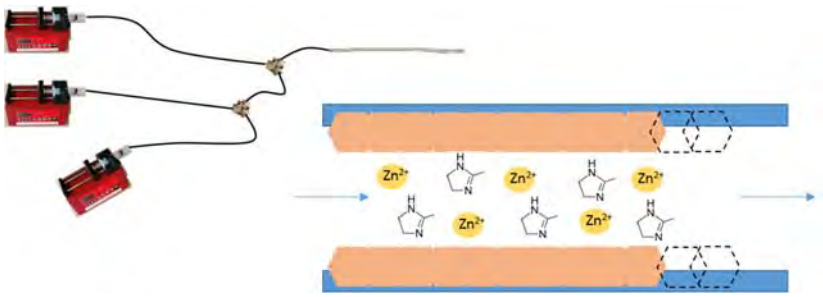

Fig. 8. *In situ* crystallization method. Metal, ligand and solvent solutions are pumped by syringe pumps through the hollow fiber lumen (blue). During the synthesis, the MOF crystallizes forming a continuous layer (pink).[24]

In this work, the authors demonstrated by FTIR, XRD and TGA the presence of both MOFs in the hollow fibers. Additionally, the ZIF hollow fibers were characterized by SEM imaging, making possible the quantification of the ZIF-8 and ZIF-7 respective thicknesses. Cacho-Bailo *et al*.[24] achieved the design of a synthesis method that allowed a better control of the layer growth. All the published techniques based on the IMMP method developed by Brown *et al*. could form ZIF-8 layers of about 8 µm, with a minimum of 5 ± 1 µm, whereas Cacho-Bailo *et al*.[24] were able to synthesize ZIF-8 and ZIF-7 layers of 3.6 ± 0.9 and 2.4 ± 0.4 µm, respectively. Interestingly, a catalytic effect was identified by TGA in the degradation of the MOF based membranes synthesized here;[115] the polysulfone membrane degraded at lower temperatures in the presence of the Zn in the MOFs.[93]

In contrast to the membranes characterized in depth by Brown *et al*.,[84] the formation of either ZIF-8 or ZIF-7 by the *in situ* procedure did not allow a sharp MOF-polymer interface to be distinguished. In fact, Cacho-Bailo *et al*.[24] evidenced the presence of MOFs inside the porosity of the support by EDS and TEM carried out on focused ion beam treated samples, concluding that a good MOF-polymer interaction was achieved.

The performance of the formed membranes was analyzed when separating binary equimolar mixtures including H_2, N_2, CO_2 and CH_4. A significant reduction in H_2 permeance in the H_2/CH_4 mixture was observed when using a bare polysulfone membrane and the synthesized ZIF-8 based membrane (52 compared to 881 GPU). The latter membrane showed separation factors of 17.2 ± 6.5, 18.3 ± 6.8 and 6.1 ± 3.2 at 35 °C when separating H_2/CH_4, H_2/N_2 and CO_2/CH_4 mixtures, respectively. The ZIF-8 based membrane was able to restrict large molecule permeances (N_2 and CH_4 with respective kinetic diameters of 3.64 and 3.8 Å), but it let smaller H_2 and CO_2 molecules diffuse (with respective kinetic diameters of 2.9 Å and 3.3 Å). In contrast,

the ZIF-7 layer showed a sharper sieving effect than ZIF-8 due to its lower pore size (3.0 Å compared to 3.4 Å, see Fig. 9). In fact, using ZIF-7, the separation factor when separating H_2/CH_4, H_2/N_2 and CO_2/CH_4 at 35 °C mixtures increased to 34.6 ± 4.0, 35.1 ± 4.3 and 13.5 ± 2.4, respectively. Nevertheless, after a study of the effect of the temperature on the performance of both membranes, the authors observed that the ZIF-8 based membrane achieved the best H_2/CH_4 separation performance at 100 °C (the separation factor increased 15% compared to the value at 35 °C) and the ZIF-7 based membrane achieved the best at 150 °C (with an increase of 119% compared to the value at 35 °C). Besides, they observed a stable and constant performance of both ZIF-8 and ZIF-7 based membranes working with a pressure gradient of up to 4 bar.[24]

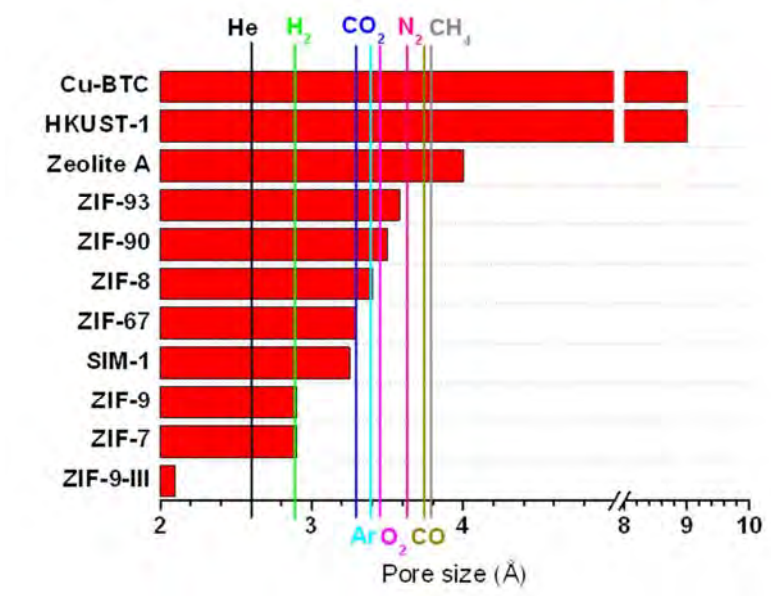

Fig. 9. MOF pore sizes and gas kinetic diameters. Zeolite A is included for comparison.

Cacho-Bailo *et al.*[22] followed the same method to synthesize ZIF-93 on the inner surface of co-polyimide P84® hollow fibers, which were more permeable than the previously used

polysulfone supports. As in the case of ZIF-8 and ZIF-7 on polysulfone, the formed hollow fibers did not show a sharp MOF-polymer interface, but an intergrowth inside the porosity of the P84® inner surface. Besides, the TGA evidenced a catalytic effect during the degradation of the ZIF-93-based hollow fiber due to the presence of the zinc.[93] According to Fig. 9, and as indicated in other publications,[116] the pore size of the ZIF-93 rho structure should distinguish between H_2 and CH_4, and even between H_2 and CO_2. In fact, the good separation performances achieved with H_2/CH_4 and CO_2/CH_4 mixtures at low temperatures (35 °C) evidenced this hypothesis (see Table 3). Besides, it was interesting to see how the performance even improved measuring the H_2/CH_4 separation at high temperature (from 60 ± 7 at 35 °C to 97 ± 6 at 100 °C) due to a good MOF-polymer affinity enhanced through an annealing effect that densified the surface microporosity of the polyimide support.[23]

In fact, Cacho-Bailo *et al*.[23] studied the effect of the annealing up to 175 °C of ZIF-8 and ZIF-93 membranes prepared by microfluidics on P84® hollow fibers. The annealing procedure was carried out while measuring the gas separation performance in terms of H_2/CH_4 separation either before the microfluidic synthesis or after such synthesis. The annealing carried out before decreased the membrane surface roughness (as analyzed by atomic force microscopy) and this worsened the MOF-polymer interaction and thus the performance of the resulting membrane, as shown in Table 4. However, the membrane prepared by microfluidics could withstand the 175 °C annealing conditions giving rise to the best separation performance. Cacho-Bailo *et al*. explained the improvement by means of a rearrangement of the polymer chains near the interface between the P84® and the MOF layer, therefore increasing the interaction and adherence between them. An additional transition temperature was observed by differential scanning calorimetry in the annealed polymer, probably due to the presence of parts of the polymer with different rigidity.

Table 4. Annealing effect in the separation performance at 35 °C of ZIF-8@P84 and ZIF-93@P84 membranes.

Annealing at 175 °C	ZIF-8				ZIF-93			
	H_2/CH_4		H_2/CO_2		H_2/CH_4		H_2/CO_2	
	H_2 (GPU)	α	H_2 (GPU)	α	H_2 (GPU)	α	H_2 (GPU)	α
Before microfluidic synthesis	46	43.5	14	20.4	12	43.5	3.0	20.4
After microfluidic synthesis	39	72.4	8.3	18.4	9.7	72.4	2.0	18.4

Focusing on pre-combustion applications, Cacho-Bailo *et al*.[26] carried out a study whose goal was to emulate with MOF based hollow fibers the recent performances achieved with flat membranes by Caro *et al*.,[117-120] Li *et al*.[121, 122] and Peng *et al*. for H_2/CO_2 separation.[123] The latter authors achieved the highest H_2/CO_2 separation factor ever achieved of 291 with exfoliated ZIF-7-III as a membrane building block. According to these authors, the nanostructures required to accomplish a good H_2/CO_2 separation must have restricted pore sizes between 3 and 5 Å, and distinctive adsorption properties, since both H_2 and CO_2 have similar kinetic diameters (see Fig. 9). The MOFs used by Cacho-Bailo *et al*. were ZIF-8, ZIF-9 and ZIF-67. ZIF-9 has a higher CO_2 adsorption capacity than the ZIF-8 and ZIF-67, while ZIF-9 has a more restrictive pore size (Fig. 9) than the other two MOFs. For this reason, Cacho-Bailo *et al*.[26] looked for a synergic effect between these three ZIFs. They sequentially synthesized by microfluidics two types of MOF-based membranes where two different MOFs were combined to obtain two-layered MOF hollow fiber membranes. ZIF-67 or ZIF-8 on the surface, exposed to the H_2/CO_2 to be separated, decreased the CO_2 adsorption tendency, favoring the selective H_2 transport, whereas the ZIF-9 enhanced the sieving effect of the two-layered membrane (see Fig. 10A). In fact, the microfluidic approach allowed the sequential synthesis of the two ZIFs creating ZIF-8/ZIF-9 or ZIF-67/ZIF-9 compact two-layered membranes of 2.0 ± 0.4 μm in thickness.

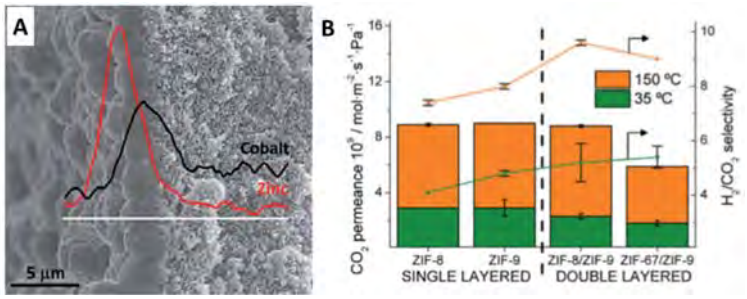

Fig. 10. EDS analysis of the presence of cobalt from ZIF-9 and zinc from ZIF-8 in the interface of a dual MOF based hollow fiber membrane (A). MOF-based membranes made of ZIF-8, ZIF-9 or combinations of them, ZIF-8/ZIF-9 and ZIF-67/ZIF-9, separating H_2/CO_2 mixtures at 35 °C and 150 °C (B)

As shown in Fig. 10A, both MOF layers could be distinguished by EDS, since Zn was present only in ZIF-8 and Co only in ZIF-9. It was interesting that even though the interface between both MOF layers was detectable by the presence of both metals, the authors hypothesized that the two MOF structures could have been interpenetrated producing some kind of hybrid structure. Other authors who synthesized ZIFs by ligand exchange have pointed this out.[124-126] Besides, Cacho-Bailo et al. achieved interesting gas separation results, since significant improvements were observed with these new membranes compared to the ZIF-8 and ZIF-9 alone (Fig. 10B), especially at 150 °C. The separation factors of the combined MOF-based membranes showed values of 9.6 ± 0.1 and 9.0 ± 0.0 for ZIF-8/ZIF-9 and ZIF-67/ZIF-9, respectively, whereas the ZIF-8 and ZIF-9 alone showed 7.4 ± 0.1 and 8.0 ± 0.1, respectively. However, the H_2 permeance was lower in the ZIF-67/ZIF-9 membrane than in the ZIF-8/ZIF-9 at 35 °C (see Table 3 and Fig. 10B for comparison) because of a slightly more limiting pore size of the ZIF-67 (see Fig. 9), although the separation factors had similar values. Besides, the temperature had a significant effect on the separation performance because the CO_2 adsorption was reduced, thus the sieving effect contribution increased: at 150 °C the H_2/CO_2 separation factors were 9.6 ± 0.1 and 9.0 ± 0.0 for ZIF-8/ZIF-9 and ZIF-67/ZIF-9, respectively, compared to 5.2 ± 0.7 and 5.4 ± 0.4 at 35 °C (see Fig 10B).[26]

Microfluidics can also be used to prepare MOF membranes in highly permeable supports, such as those made by sintering metal particles.[127] In such supports the percolation phenomenon is very intensive and Cacho-Bailo *et al*.[127, 128] had to adapt their synthesis method,[94] particularly filling the support porosity with polyether polyethylene glycol (PEG). The good compatibility between MOF and polymeric supports has been clearly demonstrated in several previous works, such as those reported by Brown *et al*., Eum *et al*. and Cacho-Bailo *et al*. However, it is well known that high temperatures and possible catalytic effects produced by MOFs limit the usefulness of polymeric membranes in some separation processes, even if the MOF stability can be high at temperatures as high as 350-400 °C, as in the case of ZIF-8.[93] In this new publication, the authors synthesized ZIF-9 phase III, with very narrow porosity (ZIF-9-III, ca. 2.1 Å, see Fig. 9) and low CO_2 adsorption capacity, on the lumen of nickel supports.[25] When these ZIF-9-III membranes on Ni metal hollow fibers were applied to separate H_2/CO_2 and He/CH_4 mixtures, He and H_2 could permeate through the membrane pores even though their kinetic diameters are larger than the small ZIF-9-III pore size (2.1 Å), thus some flexibility must be assumed in the bonds of the ZIF structure. In contrast with the results reported in other publications where low H_2/CO_2 separation factors were registered at low temperatures because of the CO_2 adsorption and condensation,[129] the ZIF-9-III membrane enhanced its separation factor when the temperature decreased, giving a H_2/CO_2 separation factor of 22.2 (102 GPU of H_2) at -10 °C. This unusually high selectivity was explained not only by the low CO_2 adsorption capacity of ZIF-9-III[26, 130] but also by the contraction of the MOF structure as the temperature decreased, due to its negative thermal expansion coefficient ($27.4 \cdot 10^{-6}$ K^{-1}).[94] The performance of this metal-supported membrane was clearly different to that observed with the polymeric-supported membranes, as highlighted with the SIM-1 (also known as ZIF-94) hollow fiber membrane on polyimide P84®, also synthesized by microfluidics. This showed the expected increase in H_2 permeance with the increase in temperature, and a maximum of H_2/CO_2 at 0 °C, related to enhanced CO_2 adsorption.[94, 131]

It is worth mentioning that the ZIF-9-III membrane was prepared upon the crystallization of the conventional ZIF-9 which was converted into ZIF-9-III by means of a hydrolysis reaction carried out by pumping water through the lumen of the hollow fiber membrane. This highlights the flexibility of microfluidics that can sequentially generate a second phase, while minimizing the risk of the membrane bursting. This approach has also been used to functionalize ZIF-94 membranes *in situ*.[132] In fact, a modification in the gas separation performance of ZIF-94 (with sod type structure) hollow fiber membranes by means of an imine-condensation functionalization reaction carried out by sequential microfluidics caused the ZIF atoms to be rearranged in a less dense rho structure (ZIF-93), with a wider pore diameter and a diminished CO_2 affinity.

4.3.3. Other methods

Biswal *et al*.[88] synthesized MOF-based membranes following an interfacial synthesis method (Fig. 11) which was used to synthesize layers of MOFs ZIF-8 and Cu-BTC MOFs either on the outer or inner sides of PBI-BuI hollow fiber supports by microfluidic means. Like other interfacial syntheses used for the formation of composite membranes (e.g. thin film composite and thin film nanocomposite membranes),[133-135] the synthesis achieved an auto-limited growth to obtain a continuous MOF layer by using two immiscible solvents. Besides, Biswal *et al*. were able to choose the surface of the hollow fiber (inner or outer) that would be covered by the MOF layer because the linker was soluble in both phases, but the metal salt only in one. As a result, both CuBTC and ZIF-8 membranes were characterized by observing different crystal sizes and shapes.[88] The different sizes could be explained by the effect of the superficial porosity of the PBI-BuI support in the interfacial synthesis, but the authors did not fully explain the presence of the different shapes. These membranes were applied to the separation of He/C_3H_8 and He/N_2 mixtures at 35 °C with modest performance (see Table 3).

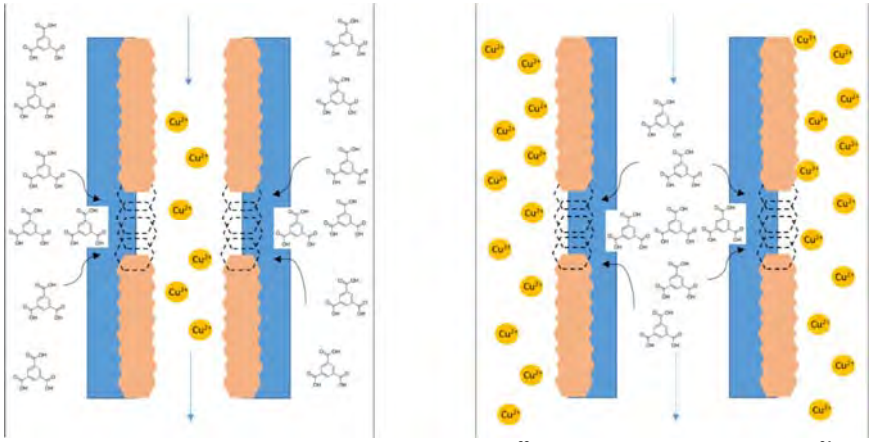

Fig. 11. Scheme of the synthesis method developed by Biswal *et al*.[88] In a similar way to the IMMP method,[84] two different solutions (metal solution and ligand solution, both of them with immiscible solvents) were located at the lumen side of a hollow fiber and at the shell side of the membrane module. By changing the location of both precursors, the MOF layer could be formed on the inner or outer surfaces of the hollow fiber.

Mao *et al*.[89] designed a synthesis method in which the metal precursor for the MOF was copper hydroxide nanostrands (CHN) and the linker was dissolved in an ethanol/water solution. The PVDF support was first pre-coated with the CHN by a filtration step of 40 min by microfluidic means, and after that the support was immersed in the solution where a synthesis of 40 min occurred. This method decreased significantly the time of the HKUST-1 formation compared to the common metal salt-linker reactions. The observed MOF film (6 µm thick) was composed of a porous layer, intergrown inside the support pores, and a dense layer of around 3 µm thickness on the support surface. When the dense layer was formed, the resistance to the linker diffusion increased and the reaction rate decreased, thus a less packed structure was formed. The effects of the linker concentration and filtration pressure were also studied, observing a faster reaction rate and better intergrowth layers at high linker concentrations and high filtration rates. The gas separation performances showed low separation factors near to the corresponding Knudsen values with relatively high hydrogen permeances.

Eum *et al*.[96] synthesized ZIF-90 with DMF on both crosslinked PVDF (c-PVDF) and macroporous carbon hollow fibers. In spite of the stability of the c-PVDF support in contact with the DMF, it tended to swell, thus its dimensions increased during the ZIF-90 synthesis. Consequently, after the post-synthesis drying process, the c-PVDF hollow fiber dimensions decreased, which produced the detachment of the MOF layer. In contrast, the carbon hollow fiber did not experience the DMF swelling phenomenon, and the ZIF-90 formed was more stable. By processing n-C_4H_{10}/i-C_4H_{10} mixtures, Eum *et al*.[96] observed a n-C_4H_{10} permeance similar to that obtained through the bare carbon fiber, even though the i-C_4H_{10} permeance decreased after forming the ZIF-90 layer. Because of this, Eum *et al*.[96] concluded that there were defects in the film, although in a low concentration. As they mentioned, previous works about ZIF-8 formation in hollow fibers showed less defective membranes,[84, 86, 95, 126] thus the issues in this case probably arose from the synthesis method. The authors hypothesized that the partial miscibility of the solvents used in the IMMP method followed here (DMF/1-octanol) may have created a less stable MOF-carbon interface than that achieved by other authors who used an immiscible pair of solvents (water/1-octanol). Besides, Eum *et al*.[96] synthesized a ZIF-8 continuous layer on the carbon hollow fiber and used the obtained membrane to dehydrate organics (furfural and ethanol) with water/organic separation factors of 1040-570 during 4 days of continuous operation.

4.4. Reactant savings

There is a general concern about the possibility of solvent reuse in the synthesis of MOFs.[136] As mentioned in previous publications about microfluidics, one of the main advantages of microfluidic synthesis is the lower usage of reactants than in common bulk synthesis. It is important to mention that some of the syntheses for MOF-based membranes mentioned above are not fully based on microfluidics fundamentals. This is the case of the IMMP method and the methods used by Biswal *et al*.[88] and Mao *et al*.[89], where only the solution pumped through the

lumen side of the hollow fiber followed a laminar regime with a low Péclet number. For this reason, the solvent and linker usages in these works were even larger than in non-microfluidic methods, as shown in Fig. 12.

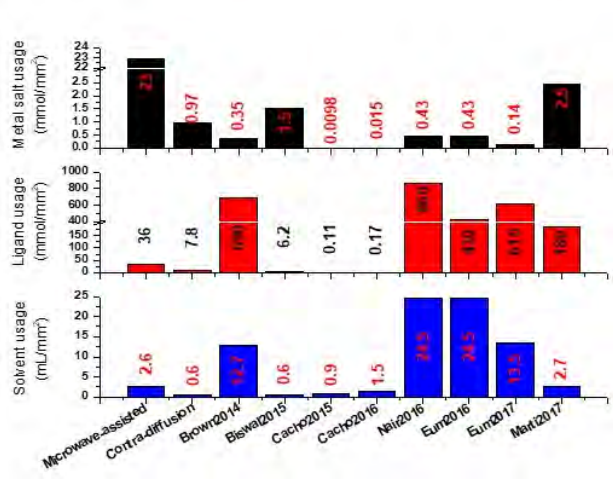

Fig. 12. Comparison in the usage of reactants for the synthesis of ZIF-8 (metal salt (A), ligand (B) and solvents (C)) between bulk crystallization and microfluidic means. Each column corresponds to (in order): Lai *et al*. (microwave-assisted synthesis),[137] Zhang *et al*. (contra-diffusion method),[138] Brown *et al*.,[84] Biswal *et al*.,[88] Cacho-Bailo *et al*.,[24] Cacho-Bailo *et al*.,[26] Eum *et al*.,[86] Eum *et al*.,[95] Eum *et al*.[96] and Marti *et al*.[114]

The usage of reactants for bulk synthesis that appear in the figure above corresponds to the studies published by Lai *et al*.[137] and Zhang *et al*.[138] Among all the works published in this field, these two were selected for comparison with the microfluidic based syntheses because both of them use energy-efficient synthesis methods. The comparison in Fig. 12 only refers to the usage of metal salts, ligand and solvent in the synthesis of continuous ZIF-8 layers on different supports (flat membranes and hollow fibers made of either inorganic or polymeric materials), but other parameters should be taken into account such as reaction time and temperature.

The IMMP method, used by Brown *et al*.[84] and by Eum *et al*.,[86, 95, 96] uses relatively high quantities of solvents and ligand per membrane area unit (mm^2). In contrast, the metal salt amounts are extremely low because during 420 min out of the total 560 min of synthesis time, the metal salt solution remained stagnant. Besides, Eum *et al*.,[95] optimized the IMMP method synthesis conditions by reducing the ligand concentration to half the original value. Cacho-Bailo *et al*.[24] substantially reduced the usage of reactants when preparing ZIF membranes on polysulfone because their method was only based on microfluidics. Besides, the synthesis time was significantly lower than in the IMMP (2.5 h compared to 9.3 h). Nevertheless, the quantity of reactants per membrane area unit was higher when using polyimide P84® supports because they maintained the same synthesis parameters (concentration and flow), but the P84® hollow fiber inner surface area was lower.[26] Finally, Biswal *et al*.[88] designed a method where the usage of reactants is relatively low due to the fact they synthesized ten ZIF-8 hollow fiber membranes at the same time.

Lai *et al*.[137] carried out the synthesis of a continuous layer of ZIF-8 on the surface of an α-alumina support by a seeding and microwave-assisted secondary growth. Interestingly, the ligand and solvent usages in this work were lower than in the IMMP method (see Fig. 12), even though Lai et al.[137] used a bulk synthesis divided in two stages (seeding and secondary growth). This is due to the fact that in the IMMP a large quantity of reactants was deposited at the shell side of the membrane module, although the usage of metal salt was significantly lower in the IMMP method because it was pumped through the lumen side of the hollow fiber membrane. However, it is important to mention that from the energy efficiency point of view the bulk synthesis of Lai *et al*. had significant drawbacks, since it needed between 7 and 8 h, and the procedure took place at high temperature conditions. In contrast, Cacho-Bailo *et al*.[24] needed only 2 h for the synthesis of ZIF-8 at room temperature. Besides, the microfluidic methods in general offer a better control of MOF layer thickness. Lai *et al*.[137] synthesized a ZIF-8 film of

about 50 µm thick, while any microfluidic based membranes synthesis achieves about 10 µm of thickness as maximum (see Table S1).

Zhang *et al*.[138] did achieve a very precise control of the ZIF-8 layer synthesis by obtaining a thickness of about 550 nm. They used a contra-diffusion method based on several previous works that was optimized by the development of a tailor-made membrane which consisted of a thin polydopamine-wrapped single-walled carbon nanotube (PD/SWCNT) structure.[84, 104, 139] The optimization lay in the pore size of such supports which was about 5-10 nm, smaller than the 100 nm used in previous works. As can be seen in Fig. 12, the reactants usage in the Zhang *et al*.[138] method was very close to that used in microfluidics synthesis. In fact, this is one of the methods that needed the lowest amount of solvent to carry out the synthesis of ZIF-8, although the metal salt and ligand usages were relatively high.[24] Nevertheless, this synthesis took 24 h at room temperature to finish, a time period dramatically reduced in microfluidic methods.

5. Conclusions and outlook

Metal-organic frameworks (MOFs) are a class of crystalline porous materials which has emerged in competition to zeolites. Zeolites are thermally and chemically more stable but MOFs have additional advantages such as their organic-inorganic character, flexible structure and easier design. To date, MOF applications have included catalysts,[140] luminescent materials,[141] drug delivery,[142] sensing and electronic devices,[143] water treatment,[144] gas separation,[145] gas storage[146] and heat transformation.[147] Therefore, it is not surprising that industrial applications of MOFs have been predicted several times in recent years.[148, 149] In fact, some MOFs are on the market and recently the first commercial product with MOFs for the release of gases for the semiconductor industry has been launched.[150] However, further efforts are required to expand the market for both new materials and synthesis procedures.

The global microfluidics market is predicted to reach USD 8.78 billion by 2021, at a compound annual growth rate of 19.2% from 2016 to 2021.[151] In this context, and as shown in

Comentado [JC3]: He añadido esto, poner esta referencia reciente publicada en Science:
Defibrillation of soft porous metal-organic frameworks with electric fields

the present review, the interest in microfluidics for the synthesis of MOFs is undeniable given its operational characteristics such as simplicity, low sizes, short times, continuous operation and enhanced transport properties. As has been shown, these characteristics make the process controllable, scalable, reproducible and allow the preparation of complex, advanced and functional structures including nanoparticles of uniform size and thin films. In addition, compared to traditional methods, microfluidic synthesis is environmentally friendly regarding the consumption of reagents and energy saving, with low carbon footprints and a high degree of safety. Several MOFs particles (NH_2-MIL-88B, MIL-88B, Br-MIL-88B, ZIF-8, HKUST-1, MOF-5, IRMOF-3 and UiO-66)[13, 56, 60, 64] have been prepared to date using the different microfluidic techniques examined in this review (segmented microfluidics, digital microfluidic systems and synthesis in microdroplets).[13, 56, 60, 64, 68, 72, 73] Besides, different hierarchical structures, such as yolk/shell MOF/polymer and MOF hollow spheres for enzyme encapsulation,[79] and the direct functionalization of MOFs with desired functional groups[72] have been prepared and carried out with microfluidic techniques. Of course, other MOFs and new related materials will be welcome additions for the newly developed microfluidic technology, for example its recent use for COFs.[152]

The importance of separation processes in industry must be taken into account since, for example, industrial separation processes account for approximately 10–15% of the total energy consumption in the United States.[91] The use of membranes as a separation technology of low energy consumption can considerably reduce this proportion. Among the major problems of many types of membranes are the permeability/selectivity trade-off and their scaling and reproducibility from laboratory conditions to industrial scale production. Therefore, the development of appropriate materials and synthesis procedures continues to be necessary. As discussed during this review, the exceptional properties of MOFs and the invaluable help of microfluidics in the preparation of scalable and reproducible hollow fibers with intrinsically low carbon footprints can aid the development of highly intensified, more effective and more

efficient membrane processes. Such development is environmentally friendly and, of course, the separation processes to which membranes can be applied (e.g. CO_2 capture, biogas upgrading and hydrogen purification) are related to issues of the environment and sustainability. In this review, we have analyzed different microfluidic techniques[24, 84, 88] for the preparation of hollow fibers to obtain diverse MOFs layers (ZIF-7, ZIF-8, ZIF-9, ZIF-67, ZIF-90, ZIF-93, SIM-1, ZIF-9-III, HKUST-1 and Cu-BTC).[22-24, 26, 84, 86, 88, 89, 94-96] The microfluidic techniques have been shown to provide very versatile syntheses and double layers of MOFs,[26] sequential modification,[94] and the functionalization of membranes.[132]

In addition, microfluidic technology developed for MOF membranes used in gas separation will be applicable to other separation techniques such as pervaporation and nanofiltration, and of course to other related fields of interest using films (microchromatography, sensors, microreactors, health and biotechnology, among others).[96]

In any event, it is not only the development of materials and synthesis methods that should be considered for the advance of microfluidic synthesis, but also detailed characterization which is the key to a complete understanding of advanced nanostructured materials. Further progress in process design through modeling and simulation avoiding heuristic approaches would also be welcome. Moreover, the combination of microfluidics with other techniques (e.g. microwave synthesis presented as an interesting efficient method for large scale production of MOFs) may give rise to remarkable improvements.[153] And, very importantly, it is desirable to increase the throughput and the scale-up of the process, which in principle should be simple with parallelization.[154] Taking all these factors into account, the synthesis of MOFs by microfluidics could be economically and environmentally competitive for commercial production compared to traditional processes.

Acknowledgements

Financial support from the Spanish MINECO and FEDER (MAT2016-77290-R), the Aragón Government (T05) and the ESF is gratefully acknowledged. C. E.-G. thanks the Aragón Government for his PhD grant.

6. Bibliography

1. G. Ferey, *Chemical Society Reviews*, 2008, **37**, 191-214.
2. J. L. C. Rowsell and O. M. Yaghi, *Microporous Mesoporous Mat.*, 2004, **73**, 3-14.
3. D. Farrusseng, S. Aguado and C. Pinel, *Angew. Chem.-Int. Edit.*, 2009, **48**, 7502-7513.
4. D. J. Tranchemontagne, J. L. Mendoza-Cortes, M. O'Keeffe and O. M. Yaghi, *Chemical Society Reviews*, 2009, **38**, 1257-1283.
5. M. I. Nandasiri, S. R. Jambovane, B. P. McGrail, H. T. Schaef and S. K. Nune, *Coord. Chem. Rev.*, 2016, **311**, 38-52.
6. L. Sun, M. G. Campbell and M. Dinca, *Angew. Chem.-Int. Edit.*, 2016, **55**, 3566-3579.
7. F. X. Coudert and A. H. Fuchs, *Coord. Chem. Rev.*, 2016, **307**, 211-236.
8. B. Seoane, S. Castellanos, A. Dikhtiarenko, F. Kapteijn and J. Gascon, *Coord. Chem. Rev.*, 2016, **307**, 147-187.
9. M. Gimenez-Marques, T. Hidalgo, C. Serre and P. Horcajada, *Coord. Chem. Rev.*, 2016, **307**, 342-360.
10. P. Horcajada, R. Gref, T. Baati, P. K. Allan, G. Maurin, P. Couvreur, G. Ferey, R. E. Morris and C. Serre, *Chem. Rev.*, 2012, **112**, 1232-1268.
11. S. K. Henninger, H. A. Habib and C. Janiak, *Journal of the American Chemical Society*, 2009, **131**, 2776-+.
12. M. Rubio-Martinez, T. D. Hadley, M. P. Batten, K. Constanti-Carey, T. Barton, D. Marley, A. Monch, K. S. Lim and M. R. Hill, *ChemSusChem*, 2016, **9**, 938-941.
13. L. Paseta, B. Seoane, D. Julve, V. Sebastian, C. Tellez and J. Coronas, *Acs Applied Materials & Interfaces*, 2013, **5**, 9405-9410.
14. M. Rubio-Martinez, C. Avci-Camur, A. W. Thornton, I. Imaz, D. Maspoch and M. R. Hill, *Chemical Society Reviews*, 2017, **46**, 3453-3480.
15. P. Falcaro, D. Buso, A. J. Hill and C. M. Doherty, *Adv. Mater.*, 2012, **24**, 3153-3168.
16. P. A. Julien, C. Mottillo and T. Friscic, *Green Chem.*, 2017, **19**, 2729-2747.
17. A. J. Howarth, A. W. Peters, N. A. Vermeulen, T. C. Wang, J. T. Hupp and O. K. Farha, *Chemistry of Materials*, 2017, **29**, 26-39.
18. N. A. Khan and S. H. Jhung, *Coord. Chem. Rev.*, 2015, **285**, 11-23.
19. S. L. Qiu, M. Xue and G. S. Zhu, *Chemical Society Reviews*, 2014, **43**, 6116-6140.
20. J. Klinowski, F. A. A. Paz, P. Silva and J. Rocha, *Dalton Transactions*, 2011, **40**, 321-330.
21. O. K. Farha and J. T. Hupp, *Accounts Chem. Res.*, 2010, **43**, 1166-1175.
22. F. Cacho-Bailo, G. Caro, M. Etxeberria-Benavides, O. Karvan, C. Tellez and J. Coronas, *Chemical Communications*, 2015, **51**, 11283-11285.
23. F. Cacho-Bailo, G. Caro, M. Etxeberria-Benavides, O. Karvan, C. Tellez and J. Coronas, *Rsc Advances*, 2016, **6**, 5881-5889.
24. F. Cacho-Bailo, S. Catalan-Aguirre, M. Etxeberria-Benavides, O. Karvan, V. Sebastian, C. Tellez and J. Coronas, *Journal of Membrane Science*, 2015, **476**, 277-285.
25. F. Cacho-Bailo, M. Etxeberria-Benavides, O. David, C. Tellez and J. Coronas, *ACS Appl. Mater. Interfaces*, 2017, **9**, 20787-20796.
26. C.-B. Fernando, I. Matito-Martos, J. Perez-Carbajo, M. Etxeberría-Benavides, K. Oguz, V. Sebastián, S. Calero, C. Téllez and J. Coronas, *Chem. Sci.*, 2016.

27. J. Y. Zhang, C. H. Gong, X. H. Zeng and J. L. Xie, *Coord. Chem. Rev.*, 2016, **324**, 39-53.
28. J. M. Wang and Y. J. Song, *Small*, 2017, **13**, 19.
29. M. P. Batten, M. Rubio-Martinez, T. Hadley, K. C. Carey, K. S. Lim, A. Polyzos and M. R. Hill, *Current Opinion in Chemical Engineering*, 2015, **8**, 55-59.
30. P. W. Dunne, E. Lester and R. I. Walton, *Reaction Chemistry & Engineering*, 2016, **1**, 352-360.
31. X. Y. Chen and J. N. Shen, *Journal of Chemical Technology and Biotechnology*, 2017, **92**, 271-282.
32. A. Manz, D. J. Harrison, E. Verpoorte and H. M. Widmer, *Adv. Chromatogr.*, 1993, **33**, 1-66.
33. R. Srinivasan, S. L. Firebaugh, I. M. Hsing, J. Ryley, M. P. Harold, K. F. Jensen, M. A. Schmidt and Ieee, *Transducers 97 - 1997 International Conference on Solid-State Sensors and Actuators, Digest of Technical Papers, Vols 1 and 2*, 1997, 163-166.
34. K. S. Elvira, X. C. I. Solvas, R. C. R. Wootton and A. J. deMello, *Nat. Chem.*, 2013, **5**, 905-915.
35. S. Kitagawa, R. Kitaura and S. Noro, *Angew. Chem.-Int. Edit.*, 2004, **43**, 2334-2375.
36. P. Horcajada, T. Chalati, C. Serre, B. Gillet, C. Sebrie, T. Baati, J. F. Eubank, D. Heurtaux, P. Clayette, C. Kreuz, J. S. Chang, Y. K. Hwang, V. Marsaud, P. N. Bories, L. Cynober, S. Gil, G. Ferey, P. Couvreur and R. Gref, *Nat. Mater.*, 2010, **9**, 172-178.
37. E. Koohsaryan and M. Anbia, *Chin. J. Catal.*, 2016, **37**, 447-467.
38. J. Gascon, F. Kapteijn, B. Zornoza, V. Sebastian, C. Casado and J. Coronas, *Chemistry of Materials*, 2012, **24**, 2829-2844.
39. C. S. Cundy and P. A. Cox, *Chem. Rev.*, 2003, **103**, 663-701.
40. P. M. Slangen, J. C. Jansen and H. vanBekkum, *Microporous Mater.*, 1997, **9**, 259-265.
41. C. S. Cundy and P. A. Cox, *Microporous Mesoporous Mat.*, 2005, **82**, 1-78.
42. T. Razzaq and C. O. Kappe, *Chem.-Asian J.*, 2010, **5**, 1274-1289.
43. J. X. Ju, C. F. Zeng, L. X. Zhang and N. P. Xu, *Chemical Engineering Journal*, 2006, **116**, 115-121.
44. Y. C. Pan, J. F. Yao, L. X. Zhang and N. P. Xu, *Industrial & Engineering Chemistry Research*, 2009, **48**, 8471-8477.
45. P. H. Hoang, H. Park and D. P. Kim, *Journal of the American Chemical Society*, 2011, **133**, 14765-14770.
46. L. Yu, Y. C. Pan, C. Q. Wang and L. X. Zhang, *Chemical Engineering Journal*, 2013, **219**, 78-85.
47. Z. D. Liu, T. Wakihara, D. Nishioka, K. Oshima, T. Takewaki and T. Okubo, *Chemistry of Materials*, 2014, **26**, 2327-2331.
48. J. Puigmarti-Luis, M. Rubio-Martinez, U. Hartfelder, I. Imaz, D. Maspoch and P. S. Dittrich, *Journal of the American Chemical Society*, 2011, **133**, 4216-4219.
49. T. Chalati, P. Horcajada, R. Gref, P. Couvreur and C. Serre, *J. Mater. Chem.*, 2011, **21**, 2220-2227.
50. M. Schlesinger, S. Schulze, M. Hietschold and M. Mehring, *Microporous Mesoporous Mat.*, 2010, **132**, 121-127.
51. D. F. Lv, Y. W. Chen, Y. J. Li, R. F. Shi, H. X. Wu, X. J. Sun, J. Xiao, H. X. Xi, Q. B. Xia and Z. Li, *J. Chem. Eng. Data*, 2017, **62**, 2030-2036.
52. J. S. Choi, W. J. Son, J. Kim and W. S. Ahn, *Microporous Mesoporous Mat.*, 2008, **116**, 727-731.
53. W. J. Son, J. Kim and W. S. Ahn, *Chemical Communications*, 2008, 6336-6338.
54. Z. X. Zhao, X. L. Ma, Z. Li and Y. S. Lin, *Journal of Membrane Science*, 2011, **382**, 82-90.
55. M. Faustini, J. Kim, W.-S. Ahn and K. D. Pyo, *Journal*, 2012.
56. M. Faustini, J. Kim, G. Y. Jeong, J. Y. Kim, H. R. Moon, W. S. Ahn and D. P. Kim, *Journal of the American Chemical Society*, 2013, **135**, 14619-14626.

57. J. Huo, M. Brightwell, S. El Hankari, A. Garai and D. Bradshaw, *Journal of Materials Chemistry A*, 2013, **1**, 15220-15223.
58. W. B. Yuan, A. L. Garay, A. Pichon, R. Clowes, C. D. Wood, A. I. Cooper and S. L. James, *Crystengcomm*, 2010, **12**, 4063-4065.
59. J. L. C. Rowsell and O. M. Yaghi, *Journal of the American Chemical Society*, 2006, **128**, 1304-1315.
60. A. Polyzoidis, T. Altenburg, M. Schwarzer, S. Loebbecke and S. Kaskel, *Chemical Engineering Journal*, 2016, **283**, 971-977.
61. Y. R. Lee, M. S. Jang, B. Y. Cho, H. J. Kwon, S. Kim and W. S. Ahn, *Chemical Engineering Journal*, 2015, **271**, 276-280.
62. V. V. Butova, A. P. Budnik, E. A. Bulanova and A. V. Soldatov, *Mendeleev Commun.*, 2016, **26**, 43-44.
63. H. M, J. MS, C. HY, K. HJ, K. S and A. WS, *Chem. Eng. J*, 2014, **184**, 55-60.
64. O. Kolmykov, J. M. Commenge, H. Alem, E. Girot, K. Mozet, G. Medjandi and R. Schneider, *Materials & Design*, 2017, **122**, 31-41.
65. K. S. Lin, A. K. Adhikari, C. N. Ku, C. L. Chiang and H. Kuo, *Int. J. Hydrog. Energy*, 2012, **37**, 13865-13871.
66. Y. K. Seo, G. Hundal, I. T. Jang, Y. K. Hwang, C. H. Jun and J. S. Chang, *Microporous Mesoporous Mat.*, 2009, **119**, 331-337.
67. C. Carbonell, K. C. Stylianou, J. Hernando, E. Evangelio, S. A. Barnett, S. Nettikadan, I. Imaz and D. Maspoch, *Nat. Commun.*, 2013, **4**, 7.
68. D. Witters, N. Vergauwe, R. Ameloot, S. Vermeir, D. De Vos, R. Puers, B. Sels and J. Lammertyn, *Adv. Mater.*, 2012, **24**, 1316-1320.
69. P. Kumar, A. K. Paul and A. Deep, *Microporous Mesoporous Mat.*, 2014, **195**, 60-66.
70. P. Davydovskaya, A. Ranft, B. V. Lotsch and R. Pohle, *Anal. Chem.*, 2014, **86**, 6948-6958.
71. A. Ranft, F. Niekiel, I. Pavlichenko, N. Stock and B. V. Lotsch, *Chemistry of Materials*, 2015, **27**, 1961-1970.
72. S. R. Jambovane, S. K. Nune, R. T. Kelly, B. P. McGrail, Z. M. Wang, M. I. Nandasiri, S. Katipamula, C. Trader and H. T. Schaef, *Scientific Reports*, 2016, **6**, 9.
73. A. Carne-Sanchez, I. Imaz, M. Cano-Sarabia and D. Maspoch, *Nat. Chem.*, 2013, **5**, 203-211.
74. V. Sebastian, I. Diaz, C. Tellez, J. Coronas and J. Santamaria, *Adv. Funct. Mater.*, 2008, **18**, 1314-1320.
75. M. Hartmann, A. G. Machoke and W. Schwieger, *Chemical Society Reviews*, 2016, **45**, 3313-3330.
76. B. J. Zhang, S. A. Davis and S. Mann, *Chemistry of Materials*, 2002, **14**, 1369-1375.
77. B. Seoane, A. Dikhtiarenko, A. Mayoral, C. Tellez, J. Coronas, F. Kapteijn and J. Gascon, *Crystengcomm*, 2015, **17**, 1693-1700.
78. R. Ameloot, F. Vermoortele, W. Vanhove, M. B. J. Roeffaers, B. F. Sels and D. E. De Vos, *Nat. Chem.*, 2011, **3**, 382-387.
79. G. Y. Jeong, R. Ricco, K. Liang, J. Ludwig, J. O. Kim, P. Falcaro and D. P. Kim, *Chemistry of Materials*, 2015, **27**, 7903-7909.
80. A. J. Zhang, X. Y. Li, S. Y. Zhang, Z. K. Yu, X. M. Gao, X. R. Wei, Z. X. Wu, W. D. Wu and X. D. Chen, *J Colloid Interf Sci*, 2017, **506**, 1-9.
81. R. W. Baker, *Membrane Technology and Applications*, Wiley, California, USA, 2º edn., 2000.
82. C. Zhang and W. J. Koros, *J Phys Chem Lett*, 2015, **6**, 3841-3849.
83. D. E. Sanders, Z. P. Smith, R. L. Guo, L. M. Robeson, J. E. McGrath, D. R. Paul and B. D. Freeman, *Polymer*, 2013, **54**, 4729-4761.
84. A. J. Brown, N. A. Brunelli, K. Eum, F. Rashidi, J. R. Johnson, W. J. Koros, C. W. Jones and S. Nair, *Science*, 2014, **345**, 72-75.

85. K. Eum, C. Ma, A. Rownaghi, C. W. Jones and S. Nair, *ACS Appl. Mater. Interfaces*, 2016, **8**, 25337-25342.
86. K. Eum, A. Rownaghi, D. Choi, R. R. Bhave, C. W. Jones and S. Nair, *Adv. Funct. Mater.*, 2016, **26**, 5011-5018.
87. A. M. Marti, W. Wickramanayake, G. Dahe, A. Sekizkardes, T. L. Bank, D. P. Hopkinson and S. R. Venna, *ACS Appl. Mater. Interfaces*, 2017, **9**, 5678-5682.
88. B. P. Biswal, A. Bhaskar, R. Banerjee and U. K. Kharul, *Nanoscale*, 2015, **7**, 7291-7298.
89. Y. Y. Mao, J. W. Li, W. Cao, Y. L. Ying, L. W. Sun and X. S. Peng, *Acs Applied Materials & Interfaces*, 2014, **6**, 4473-4479.
90. D. L. Gin and R. D. Noble, *Science*, 2011, **332**, 674-676.
91. D. S. Sholl and R. P. Lively, *Nature*, 2016, **532**, 435-437.
92. W. J. Koros and R. P. Lively, *Aiche J.*, 2012, **58**, 2624-2633.
93. F. Cacho-Bailo, C. Tellez and J. Coronas, *Chem.-Eur. J.*, 2016, **22**, 9533-9536.
94. F. Cacho-Bailo, M. Etxeberria-Benavides, O. David, C. Tellez and J. Coronas, *Acs Applied Materials & Interfaces*, 2017, **9**, 20787-20796.
95. K. Eum, C. Ma, A. Rownaghi, C. W. Jones and S. Nair, *Acs Applied Materials & Interfaces*, 2016, **8**, 25337-25342.
96. K. Eum, C. Ma, D. Y. Koh, F. Rashidi, Z. Li, C. W. Jones, R. P. Lively and S. Nair, *Adv. Mater. Interfaces*, 2017, **4**, 6.
97. M. Arnold, P. Kortunov, D. J. Jones, Y. Nedellec, J. Karger and J. Caro, *Eur. J. Inorg. Chem.*, 2007, 60-64.
98. H. Bux, F. Y. Liang, Y. S. Li, J. Cravillon, M. Wiebcke and J. Caro, *Journal of the American Chemical Society*, 2009, **131**, 16000-+.
99. J. Cravillon, S. Munzer, S. J. Lohmeier, A. Feldhoff, K. Huber and M. Wiebcke, *Chemistry of Materials*, 2009, **21**, 1410-1412.
100. Y. Y. Liu, Z. F. Ng, E. A. Khan, H. K. Jeong, C. B. Ching and Z. P. Lai, *Microporous Mesoporous Mat.*, 2009, **118**, 296-301.
101. L. X. Li, J. F. Yao, R. Z. Chen, L. He, K. Wang and H. T. Wang, *Microporous Mesoporous Mat.*, 2013, **168**, 15-18.
102. N. Hara, M. Yoshimune, H. Negishi, K. Haraya, S. Hara and T. Yamaguchi, *Journal of Membrane Science*, 2014, **450**, 215-223.
103. A. Centrone, Y. Yang, S. Speakman, L. Bromberg, G. C. Rutledge and T. A. Hatton, *Journal of the American Chemical Society*, 2010, **132**, 15687-15691.
104. J. F. Yao, D. H. Dong, D. Li, L. He, G. S. Xu and H. T. Wang, *Chemical Communications*, 2011, **47**, 2559-2561.
105. M. Meilikhov, K. Yusenko, E. Schollmeyer, C. Mayer, H. J. Buschmann and R. A. Fischer, *Dalton Transactions*, 2011, **40**, 4838-4841.
106. S. R. Venna and M. A. Carreon, *Journal of the American Chemical Society*, 2010, **132**, 76-+.
107. S. Aguado, C. H. Nicolas, V. Moizan-Basle, C. Nieto, H. Amrouche, N. Bats, N. Audebrand and D. Farrusseng, *New Journal of Chemistry*, 2011, **35**, 41-44.
108. G. S. Xu, J. F. Yao, K. Wang, L. He, P. A. Webley, C. S. Chen and H. T. Wang, *Journal of Membrane Science*, 2011, **385**, 187-193.
109. A. J. Brown, J. R. Johnson, M. E. Lydon, W. J. Koros, C. W. Jones and S. Nair, *Angewandte Chemie-International Edition*, 2012, **51**, 10615-10618.
110. W. B. Li, Z. H. Yang, G. L. Zhang, Z. Fan, Q. Meng, C. Shen and C. J. Gao, *Journal of Materials Chemistry A*, 2014, **2**, 2110-2118.
111. Y. Y. Xu, L. F. Xu, S. D. Qi, Y. L. Dong, Z. U. Rahman, H. L. Chen and X. G. Chen, *Anal. Chem.*, 2013, **85**, 11369-11375.
112. L. M. Li, F. Yang, H. F. Wang and X. P. Yan, *J. Chromatogr. A*, 2013, **1316**, 97-103.
113. L. Q. Yu, C. X. Yang and X. P. Yan, *J. Chromatogr. A*, 2014, **1343**, 188-194.

114. A. M. Marti, W. Wickramanayake, G. Dahe, A. Sekizkardes, T. L. Bank, D. P. Hopkinson and S. R. Venna, *Acs Applied Materials & Interfaces*, 2017, **9**, 5678-5682.
115. R. Z. Jin, Z. Bian, J. Z. Li, M. X. Ding and L. X. Gao, *Dalton Transactions*, 2013, **42**, 3936-3940.
116. K. G. Ray, D. L. Olmsted, J. M. R. Burton, Y. Houndonougbo, B. B. Laird and M. Asta, *Chemistry of Materials*, 2014, **26**, 3976-3985.
117. A. S. Huang, Y. F. Chen, N. Y. Wang, Z. Q. Hu, J. W. Jiang and J. Caro, *Chemical Communications*, 2012, **48**, 10981-10983.
118. A. S. Huang and J. Caro, *Angew. Chem.-Int. Edit.*, 2011, **50**, 4979-4982.
119. N. Y. Wang, Y. Liu, Z. W. Qiao, L. Diestel, J. Zhou, A. S. Huang and J. Caro, *Journal of Materials Chemistry A*, 2015, **3**, 4722-4728.
120. Y. S. Li, F. Y. Liang, H. G. Bux, W. S. Yang and J. Caro, *Journal of Membrane Science*, 2010, **354**, 48-54.
121. W. B. Li, G. L. Zhang, C. Y. Zhang, Q. Meng, Z. Fan and C. J. Gao, *Chemical Communications*, 2014, **50**, 3214-3216.
122. W. B. Li, P. C. Su, G. L. Zhang, C. Shen and Q. Meng, *Journal of Membrane Science*, 2015, **495**, 384-391.
123. Y. Peng, Y. S. Li, Y. J. Ban, H. Jin, W. M. Jiao, X. L. Liu and W. S. Yang, *Science*, 2014, **346**, 1356-1359.
124. J. A. Thompson, C. R. Blad, N. A. Brunelli, M. E. Lydon, R. P. Lively, C. W. Jones and S. Nair, *Chemistry of Materials*, 2012, **24**, 1930-1936.
125. J. A. Thompson, J. T. Vaughn, N. A. Brunelli, W. J. Koros, C. W. Jones and S. Nair, *Microporous Mesoporous Mat.*, 2014, **192**, 43-51.
126. K. Eum, K. C. Jayachandrababu, F. Rashidi, K. Zhang, J. Leisen, S. Graham, R. P. Lively, R. R. Chance, D. S. Sholl, C. W. Jones and S. Nair, *Journal of the American Chemical Society*, 2015, **137**, 4191-4197.
127. O. David, Y. Gendel and M. Wessling, *Journal of Membrane Science*, 2014, **461**, 139-145.
128. M. W. J. Luiten-Olieman, L. Winnubst, A. Nijmeijer, M. Wessling and N. E. Benes, *Journal of Membrane Science*, 2011, **370**, 124-130.
129. L. Sandstrom, E. Sjoberg and J. Hedlund, *Journal of Membrane Science*, 2011, **380**, 232-240.
130. S. Aguado, G. Bergeret, M. P. Titus, V. Moizan, C. Nieto-Draghi, N. Bats and D. Farrusseng, *New Journal of Chemistry*, 2011, **35**, 546-550.
131. S. Aguado, J. Canivet and D. Farrusseng, *Chemical Communications*, 2010, **46**, 7999-8001.
132. F. Cacho-Bailo, M. Etxeberria-Benavides, O. Karvan, C. Tellez and J. Coronas, *Crystengcomm*, 2017, **19**, 1545-1554.
133. S. Sorribas, P. Gorgojo, C. Tellez, J. Coronas and A. G. Livingston, *Journal of the American Chemical Society*, 2013, **135**, 15201-15208.
134. C. Echaide-Górriz, S. Sorribas, C. Téllez and J. Coronas, *RSC Advances*, 2016, **6**, 90417-90426.
135. J. T. Duan, Y. C. Pan, F. Pacheco, E. Litwiller, Z. P. Lai and I. Pinnau, *Journal of Membrane Science*, 2015, **476**, 303-310.
136. S. Gokpinar, T. Diment and C. Janiak, *Dalton Transactions*, 2017, **46**, 9895-9900.
137. L. S. Lai, Y. F. Yeong, K. K. Lau and A. M. Shariff, *Journal of Chemical Technology and Biotechnology*, 2017, **92**, 420-431.
138. S. X. Zhang, Z. G. Wang, H. T. Ren, F. Zhang and J. Jin, *Journal of Materials Chemistry A*, 2017, **5**, 5630-5630.
139. Y. B. Li, L. H. Wee, A. Volodin, J. A. Martens and I. F. J. Vankelecom, *Chemical Communications*, 2015, **51**, 918-920.
140. J. W. Liu, L. F. Chen, H. Cui, J. Y. Zhang, L. Zhang and C. Y. Su, *Chemical Society Reviews*, 2014, **43**, 6011-6061.

141. H. A. Habib, J. Sanchiz and C. Janiak, *Inorg Chim Acta*, 2009, **362**, 2452-2460.
142. S. Keskin and S. Kizilel, *Industrial & Engineering Chemistry Research*, 2011, **50**, 1799-1812.
143. V. Stavila, A. A. Talin and M. D. Allendorf, *Chemical Society Reviews*, 2014, **43**, 5994-6010.
144. L. Paseta, E. Simon-Gaudo, F. Gracia-Gorria and J. Coronas, *Chemical Engineering Journal*, 2016, **292**, 28-34.
145. Y. S. Bae and R. Q. Snurr, *Angew. Chem.-Int. Edit.*, 2011, **50**, 11586-11596.
146. Y. Peng, V. Krungleviciute, I. Eryazici, J. T. Hupp, O. K. Farha and T. Yildirim, *Journal of the American Chemical Society*, 2013, **135**, 11887-11894.
147. F. Jeremias, A. Khutia, S. K. Henninger and C. Janiak, *J. Mater. Chem.*, 2012, **22**, 10148-10151.
148. U. Mueller, M. Schubert, F. Teich, H. Puetter, K. Schierle-Arndt and J. Pastre, *J. Mater. Chem.*, 2006, **16**, 626-636.
149. A. U. Czaja, N. Trukhan and U. Muller, *Chemical Society Reviews*, 2009, **38**, 1284-1293.
150. T. Faust, O. Farha and B. Hernandez, *Nat. Chem.*, 2016, **8**, 990-991.
151. Marketsandmarkets: Microfluidics market by component (Microfluidic chips, micropump, microneedle), material (polymer, glass, silicon), application (genomics, proteomics, capillary electrophoresis, POC, clinical, environmental, drug delivery) - Global forecast to 2021, (accessed September 2017).
152. D. Rodriguez-San-Miguel, A. Abrishamkar, J. A. R. Navarro, R. Rodriguez-Trujillo, D. B. Amabilino, R. Mas-Balleste, F. Zamora and J. Puigmarti-Luis, *Chemical Communications*, 2016, **52**, 9212-9215.
153. M. Taddei, D. A. Steitz, J. A. van Bokhoven and M. Ranocchiari, *Chem.-Eur. J.*, 2016, **22**, 3245-3249.
154. T. W. Phillips, I. G. Lignos, R. M. Maceiczyk, A. J. deMello and J. C. deMello, *Lab Chip*, 2014, **14**, 3172-3180.

Electronic Supporting Information

New strategies based on microfluidics for the synthesis of metal organic frameworks

Carlos Echaide-Górriz,[1] Coralie Clément,[2] Fernando Cacho-Bailo,[1] Carlos Téllez[1] and Joaquín Coronas[1,*]

[1]Chemical and Environmental Engineering Department and Instituto de Nanociencia de Aragón (INA), Universidad de Zaragoza, 50018 Zaragoza, Spain

[2]Polytech Nantes, Université de Nantes, 44306 Nantes, France

*Corresponding author: Joaquín Coronas, e-mail: coronas@unizar.es.

Table S1. MOF based hollow fiber membranes synthesis parameters by microfluidics for each case.

MOF		Hollow Fiber Material	Method of Synthesis	ID (μm)	Feeding Flow (μL/min)	Residence Time (s)	Thickness (μm)	Ref
ZIF-8		Torlon	IMMP	250	1/6	1800	8.8 ± 1.4	84
ZIF-8		Torlon*[1]	IMMP*[1]	200	1	90	5 ± 1	86
ZIF-8		Torlon*[1]	IMMP*[2]	200	10	20	8.1 ± 1.6	85
ZIF-8		Torlon*[3]	IMMP*[3]	300	130	200	8.5 ± 0.5	87
ZIF-8		PBI-BuI	Interfacial synthesis	460	-	-	10 – 25	88
ZIF-8		PSf	LPE	315	100	9.4	3.6 ± 0.9	24
ZIF-7		PSf	LPE	315	100	9.4	2.4 ± 0.4	24
ZIF-8		P84	LPE	202	100	3,8	3.6 ± 0.9	23
ZIF-67		P84	LPE	202	100	3,8	1.2 ± 0.1	26
ZIF-93		P84	LPE	202	100	3.8	2.6 ± 0.4	22
ZIF-9		P84	LPE	202	100	3.8	2.4	26
ZIF-8/ZIF-9	ZIF-8	P84	LPE	202	50	4.7	2.0 ± 0.4	26
	ZIF-9	P84	LPE	202	50	4.7		
ZIF-67/ZIF-9	ZIF-67	P84	LPE	202	50	4.7	1.2 ± 0.1	26
	ZIF-9	P84	LPE	202	50	4.7		
SIM-1		P84	LPE	202	-	-	-	25
ZIF-9 (III)		Ni	LPE	480	40	0.6	-	25
CuBTC		PBI-BuI	Interfacial Synthesis	460	-	-	10 – 25	88
HKUST-1		PVDF	-	600	-	-	6.5	89
ZIF-90		Carbon	IMMP	280	10	2200	3.1 ± 0.5	96